



Stratigraphic framework for the plume mode of mantle convection and the analysis of interregional unconformities on geological maps[☆]

Anke M. Friedrich ^{*}, Hans-Peter Bunge, Stefanie M. Rieger, Lorenzo Colli, Siavash Ghelichkhan, Rainer Nerlich

Department of Earth and Environmental Sciences, Ludwig-Maximilians-University of Munich, Luisenstr. 37 and Theresienstr. 41, 80333 München, Germany



ARTICLE INFO

Article history:

Received 2 November 2016

Received in revised form 27 May 2017

Accepted 1 June 2017

Available online 10 June 2017

Keywords:

Interregional unconformities/hiatuses

Continent-scale geology

Global tectonics

Mantle convection

Mantle plume

Plume-stratigraphic maps

Stratigraphic color scheme

ABSTRACT

Mantle convection is a fundamental planetary process. Its plate mode is established and expressed by plate tectonics. Its plume mode also is established and expressed by interregional geological patterns. We developed both an event-based stratigraphic framework to illustrate the surface effects predicted by the plume model of Griffiths et al. (1989) and Griffiths and Campbell (1990) and a methodology to analyze continent-scale geological maps based on unconformities and hiatuses. The surface expression of ascending plumes lasts for tens-of-millions-of-years and rates vary over a few million years. As the plume ascends, its surface expression narrows, but increases in amplitude, leaving distinct geological and stratigraphic patterns in the geologic record, not only above the plume-head center, but also above its margins and in distal regions a few thousands-of-kilometers from the center. To visualize these patterns, we constructed sequential geological maps, chronostratigraphic sections, and hiatus diagrams. Dome-uplift with erosion (Şengör, 2001) and the flood basalts (Duncan and Richards, 1991; Ernst and Buchan, 2001a) are diagnostic starting points for plume-stratigraphic analyses. Mechanical collapse of the dome results in narrow rifting (Burke and Dewey, 1973), drainage-network reorganization (Cox, 1989), and flood-basalt eruption. In the marginal region, patterns of vertical movement, deformation and surface response are transient and complex. At first, the plume margin is uplifted together with the central region, but then it subsides as the plume ascents farther. With plume-head flattening, the plume margin experiences renewed outward-migrating surface uplift, erosion, broad crustal faulting, and drainage reorganization. Knickpoint migration occurs first inward-directed at $\frac{1}{2}$ the rate of plume ascent and later outward-directed at the rate of asthenospheric flow. Interregional-scale unconformity-bounded stratigraphic successions document the two inversions. The distal regions, which did not experience any plume-related uplift, yield complete sedimentary records of the event; Event-related time gaps (hiatuses) in the sedimentary record increase towards the center, but the event horizon is best preserved in the distal region; it may be recognized by tracing its contacts from the center outwards. We extracted system- and series-hiatuses from interregional geological maps and built hiatus maps as proxies for paleo-dynamic topography and as a basis for comparison with results from numerical models. Interregional-scale geological maps are well suited to visualize plume-related geological records of dynamic topography in continental regions. However, geological records and hiatus information at the resolution of stages will be needed at interregional scales. The plume-stratigraphic framework is event-based, interregional, but not global, with time-dependent amplitudes that are significantly larger than those of global eustatic sea-level fluctuations. Global stratigraphic syntheses require integration of plate- and plume-stratigraphic frameworks before eustatic contributions may be assessed.

© 2017 International Association for Gondwana Research. Published by Elsevier B.V. All rights reserved.

1. Introduction

One commonly accepts plate tectonics (Wilson, 1965) as a surface expression of the earth's convecting mantle (e.g., Davies and Richards,

1992; Davies, 1999). The link between plate-tectonic motion and mantle convection (Wilson, 1963) came into its own when global maps of Cenozoic and late Mesozoic plate motion (Gordon and Jurdy, 1986; Lithgow-Bertelloni and Richards, 1998) became available. These maps were instrumental in relating large-scale mantle heterogeneity to the history of plate motion and subduction (Richards and Engebretson, 1992). Their sequential assimilation into geodynamic models gave rise to mantle circulation models (Bunge et al., 1998).

Mantle convection also induces significant vertical movement of the earth's surface (e.g., Fisher, 1889; Crough, 1979; see also Fig. 1). Studies

[☆] Manuscript revised on May 14th 2017. Submitted to Gondwana Research on November 1st 2016; Special issue on passive margin processes guest editor H.-P. Bunge and U.A. Glasnacher.

* Corresponding author.

E-mail address: friedrich@lmu.de (A.M. Friedrich).

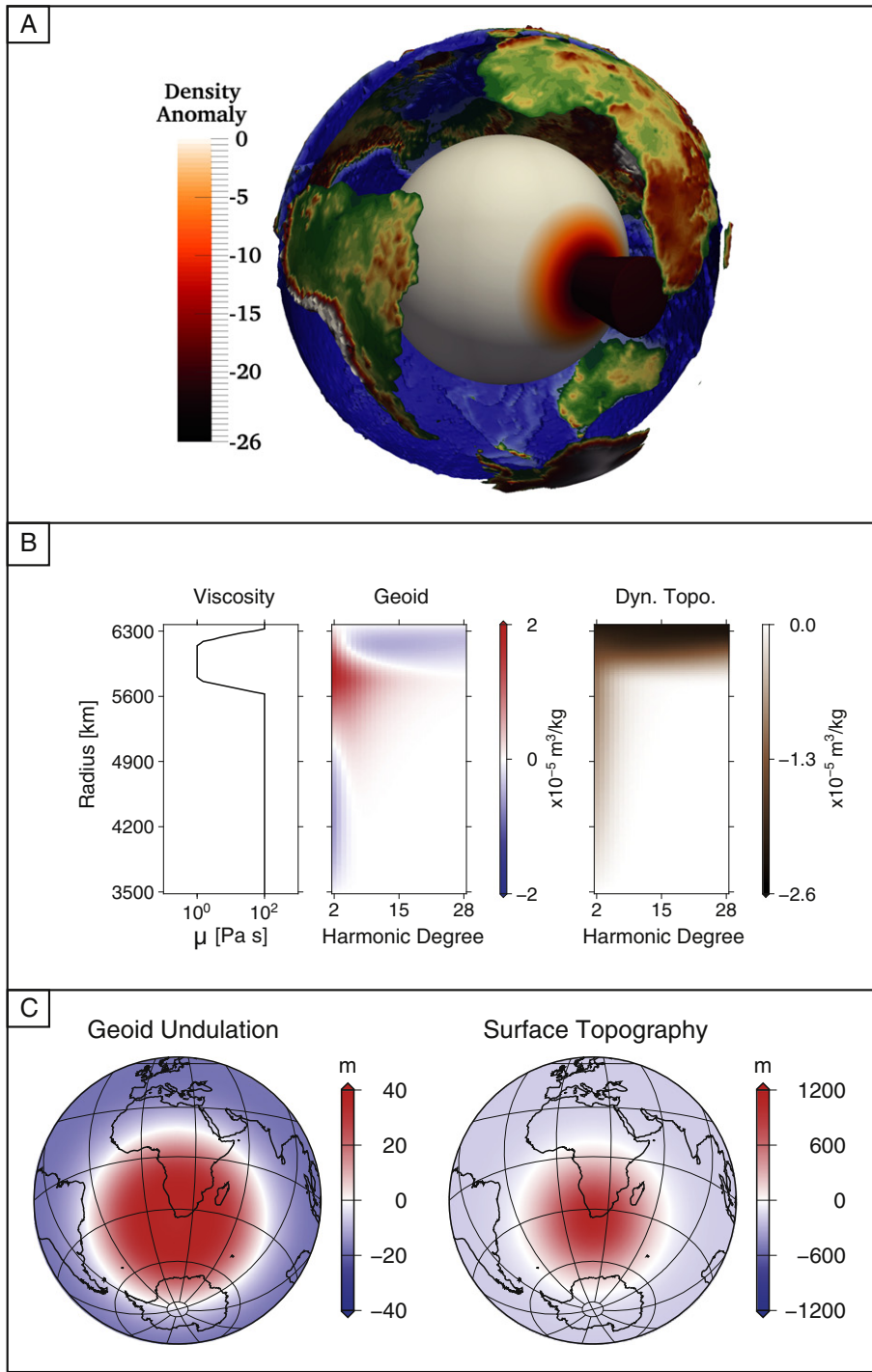


Fig. 1. Illustration of the effects of a mantle plume on geoid and dynamic topography. (A) Low seismic velocity body similar to the one inferred seismically in the lower mantle beneath Africa (Ritsema et al., 2011; French and Romanowicz, 2014), which was approximated by Colli et al. (2016) as a low density anomaly by assuming a maximum density perturbation of 26 kg/m^3 , consistent with a $250\text{--}300 \text{ K}$ thermal perturbation (Schubert et al., 2009a; Davies et al., 2015). (B) Geoid and surface dynamic topography kernels for a layered mantle viscosity profile identical to the one assumed by Colli et al. (2016). (C) Geoid undulation and surface dynamic topography induced by the assumed lower mantle density anomaly.

of gravity anomalies were performed early on in the context of viscous mantle flow, when it was realized that convective stresses in a fluid with deformable boundaries would deflect those boundaries (Morgan, 1965; McKenzie, 1977). The surface deflections of the earth's mantle are known as "dynamic topography" (Hager and Gurnis, 1987). They produce gravity anomalies of comparable amplitude to the primary mass anomalies inside the mantle. This requires taking dynamic topography into account in models of the earth's geoid (Richards and Hager, 1984; Ricard et al., 1984).

Modeling the earth's geoid with dynamic earth models has provided fundamental constraints on the mantle viscosity profile. A robust conclusion is that the upper part of the mantle has a lower viscosity than its lower part. The resolving power, however, is limited by a trade-off between the thickness of the low-viscosity upper mantle and its viscosity reduction (Schaber et al., 2009). In principle, it is possible to reduce the trade-off with information about the evolution of dynamic topography, because temporal changes of dynamic topography are tied to the mantle viscosity-profile. This can be appreciated by expressing the

topographic response of dynamic earth models through so-called “kernels” (see Colli et al., 2016, for a recent review). For a plume that rises through a uniform-viscosity mantle, the kernels predict that the surface deflection grows continuously during plume ascent, up to values of a few km. This is consistent with laboratory models of isoviscous mantle-flow (Griffiths et al., 1989). In contrast, in the presence of a weak upper mantle, much of the peak-amplitude of dynamic topography forms within a few million years, which corresponds to the vertical transit of the plume through the upper mantle. It is therefore important to map the temporal evolution of dynamic topography.

Ever since the pioneering work of Davies (1988a, 1988b), geodynamicists have been exploring mantle convection in terms of the so-called *plate*- and *plume*-modes. The former relates to cooling of the oceanic lithosphere and its subduction into the mantle, whereas the latter relates to plumes. Therefore, it is convenient to analyze dynamic topography in terms of the plate- and plume-mode. Away from active subduction zones, dynamic topography of the plate mode is large in spatial scale (10 000 km) and slowly changing in time (see Müller et al., 2018, in this issue). Its spatial scale mirrors the long-wavelength mantle-convection planform (e.g., Bunge et al., 1996), i.e., the dominance of circum-Pacific subduction in Mesozoic and Cenozoic time. Its slow temporal change was deduced by Chase and Sprowl (1983), when they noted the correspondence between major geoid lows and Cretaceous subduction, effectively suggesting that dynamic topography of the plate mode evolves on time scales of ~100 m.y. This time scale can be interpreted physically as the time needed for large-scale mantle overturn (Bunge et al., 1998).

Geologic evidence is consistent with this scale (Wilson, 1966), but it also points to episodes of shorter-lived surface uplift and subsidence, on the order of 10 m.y., at interregional scales seemingly unrelated to large-scale mantle flow of the plate mode (Ernst and Buchan, 2001a, 2001b; Şengör, 2003). These episodes reflect the plume mode of mantle flow. Their geologic expression is sometimes referred to as large wavelength structural ‘doming’ (Şengör, 2001; Guillocheau et al., 2018, in this issue). A significant plume-mode contribution to the earth’s dynamic topography is expected, because the total plume heat-transport is on the order of 10 TW (e.g., Bunge, 2005; Schubert et al., 2009a, 2009b; Simmons et al., 2009), which amounts to ~30% of the global mantle heat-budget (e.g., Davies and Davies, 2010).

Inferences on dynamic topography related to the plume mode are growing. For the North Atlantic, there are reports of repeated burial and exhumation events (e.g., Japsen et al., 2012b) and transient surface uplifts (Hartley et al., 2011; Lovell, 2010) linked to the Iceland plume. For the South Atlantic, Macgregor (2012) summarized episodes of margin uplift for South America and Africa in the Late Cretaceous and Oligocene, whereas for the Brazilian coast, Japsen et al. (2012a) document smaller-scale Late Cretaceous and Eocene burial and exhumation events that might be due to splash plumes (Davies and Bunge, 2006). Moreover, Colli et al. (2014) link South Atlantic spreading-rate changes explicitly with regional dynamic-topography changes, presumably caused by variations in pressure-driven upper-mantle flow. Maps of past dynamic-topography would link the plume mode to past mantle-convection. They would be instrumental in placing constraints on geodynamic models of the earth’s mantle flow history, derived from inverse techniques (Bunge et al., 2003; Spasojevic et al., 2009; Ghelichkhan and Bunge, 2016; Colli et al., 2018, in this issue) or backward advection (Moucha and Forte, 2011), thus greatly improving our understanding of key geodynamic modeling parameters such as the mantle viscosity profile.

The pioneering work of Campbell and Griffiths (1990) derived quantitative estimates of plume-induced surface uplift from laboratory plume models (Griffiths et al., 1989), whereas plume related surface uplift was simulated numerically by Farnetani and Richards (1994). The laboratory and numerical studies predict that the ascending plume head produces a primary 500–1000 m domal uplift. Field observations document dome-shaped uplift of 1- to 2-km over a radius of c.

1000 km (e.g., Şengör, 2001). As the plume head approaches the base of the lithosphere it flattens to form a disk, so that the dynamically-maintained topography at the plume axis decreases while it increases towards the margin. This results in subsidence above the plume axis followed by uplift towards the margin of the plume head. A volume of mantle material on order of 10^6 km^3 (Duncan and Richards, 1991) is thus fluxed horizontally beneath the lithosphere, at a rate proportional to the thickness of the disc (e.g., Campbell, 2007; Davies, 1999).

Plume-head impact at the base of the lithosphere is accompanied by dome build-up and collapse, narrow rifting, formation of giant dike swarms and the eruption of flood basalts (Burke and Wilson, 1972; Burke and Dewey, 1973; Campbell and Griffiths, 1990; Şengör, 1995; Ernst and Buchan, 2001a, and articles therein), and may lead to oceanic rifting (Courtillot et al., 1999). Here, we focus on geomorphological and stratigraphic features, which document the dynamic topographic response to plume ascent, arrival, and lateral dissipation. Ascent velocities on the order of 25–50 km/m.y. are expected (Colli et al., 2018, in this issue), whereas horizontal spreading may occur at rates as high as 200–350 km/m.y. (Hartley et al., 2011; Weismüller et al., 2015). At such rates and on these scales, the earth’s surface responds to transient vertical motion by drainage-network reorganization and erosion (Cox, 1989). Erosion of such large domal regions and over many millions-of-years requires knickpoint migration, sediment transport, and deposition in equally large regions. Therefore, numerous hiatuses and interregional unconformities are expected in stratigraphic sections and on geological maps. An upcoming challenge is to quantitatively link the geological record to dynamic topography computed by inverse geodynamic models (Colli et al., 2018, in this issue).

The purpose of our study is to develop a methodology with which to map the full extent of the surface expression of mantle plume events. We transcribed the plume-head model of Griffiths et al. (1989) and Griffiths and Campbell (1990) to an event-based plume-stratigraphic framework, and use it to analyze continent-scale geological maps. We emphasize that the model was developed for isoviscous mantle flow, whereas the earth’s mantle is layered in viscosity as noted before. The evolution of vertical surface deformation above rising mass anomalies is thus more complex, i.e., the rising history of the plume may result in dynamic topography comprising an early low-amplitude continent-scale signal and a later high-amplitude, c. 1000-km-wide dome-shaped signal. However, the focus of this paper lies on the conceptual translation of surface effects predicted by the plume mode to parameters that are quantifiable in the geological record, such as interregional hiatuses. We mapped temporal and spatial patterns of conformable and nonconformable geological contacts that surround recent large-igneous-provinces that erupted on the continents. We then plotted hiatus durations as a proxy for paleovertical motion of the earth’s surface on interregional scales, with focus on Cenozoic and Mesozoic time. Here, we merely point out the most important interdisciplinary connections and recognize that continent-scale geological maps need to be modified for this purpose. The workflow described below serves as a roadmap for future work.

2. Background materials

2.1. Mapping the expression of dynamic topography on the continents

Dynamic topography is accompanied by changes in erosion, sediment transport and deposition on interregional scales. Surface uplift associated with rising plumes is limited to a wavelength of 3000 km, an amplitude of 2 km, and a duration of millions- to tens-of-millions-of-years (see Şengör, 2003, and references therein; Burke and Wilson, 1972; Cox, 1989; Campbell, 2001; Ernst and Buchan, 2001a; Rainbird and Ernst, 2001; Şengör, 2001; Ernst and Buchan, 2002; Saunders et al., 2007; Japsen et al., 2012b). The timing of the build-up of dynamic topography depends on the details of the mantle viscosity profile, as indicated by the dynamic topography response kernels of geodynamic earth

models (Colli et al., 2016). Flood basalts have been interpreted as a surface expression of mantle plumes (e.g., Campbell and Griffiths, 1990; Courtillot et al., 1999), but interregional-scale surface uplift, expressed as long-wavelength uplift and structural doming, is the “one criterion that may be uniquely reliable in recognizing mantle plumes in the geological record” (Şengör, 2001). Şengör (2003) reviewed aspects of the history of thought and discovery of long-wavelength deformation of

the lithosphere which occurs by bending, not faulting, and without altering the rock fabric. He refers to these structures as falcogenic to avoid confusion with the term epeirogenic, which is used in numerous different ways, even though Stille (1919, 1924) defined epeirogeny as faultless up-and-down motions. Stille (1924) recognized the importance of sedimentary facies and stratigraphy in mapping interregional transgressions and regressions. He used this record to assess any

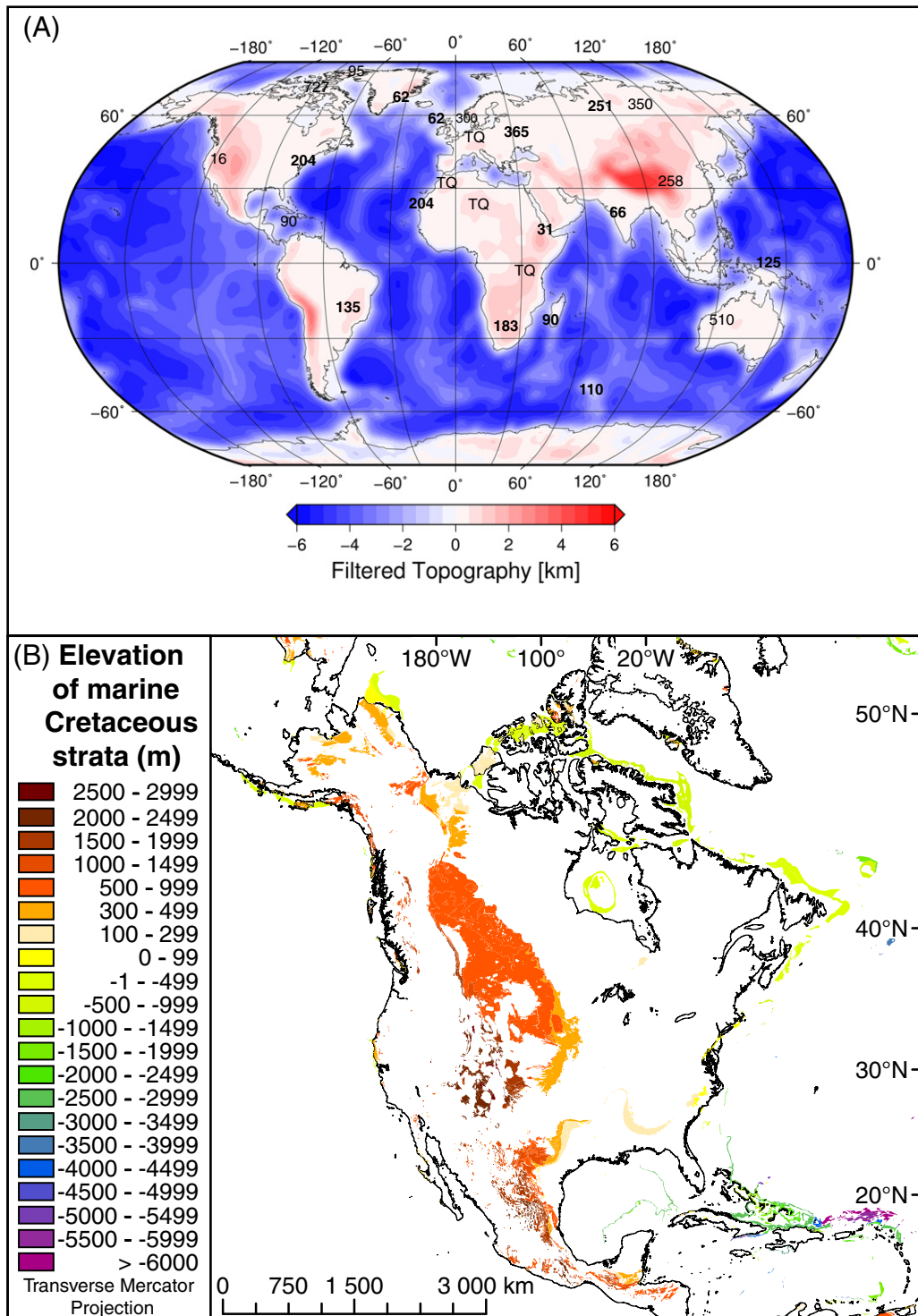


Fig. 2. (A) Map of the earth's surface showing low-frequency topography, filtered at 1000 m and taken from ETOPO1 data base (Amante and Eakins, 2009). Numbers represent locations and ages (in Ma) of major Phanerozoic continental igneous provinces, which were classified as ‘confidently linked to a plume head’ by Ernst and Buchan (2001a, 2001b). Estimated eruption volumina exceeding 1 million km³ are shown in bold. TQ — Tertiary-Quaternary mafic alkaline volcanic province. (B) Map of North America showing marine Cretaceous strata and their present-day elevation based on the International Geological Map of North America (Reed et al., 2005) with topography taken from ETOPO1 (Amante and Eakins, 2009).

temporal and regional-versus-global significance of epeirogenic motions. Soviet geologists mapped sedimentary facies and stratal thicknesses over large territories (former USSR) and over long periods of time; they perceived vertical motion of the earth's crust as more significant than its horizontal components (Belousov, 1962). They were convinced that "all manifestations of the earth's tectonic life are closely and regularly interrelated, together forming an integral process that merely changes its form in time and space" (Belousov, 1962, p. 51).

Global topographic maps filtered at a wavelength of 1000 km show numerous large plateau-like regions with average elevations well over 1000 m far inland from plate boundaries (Fig. 2A). These regions are currently undergoing uplift and erosion and are associated with large-igneous-provinces that are "confidently linked to a plume head" (Category A of Ernst and Buchan, 2001b) based on criteria such as voluminous mafic magmatism, short eruption duration, linkage to present-day hot spot, or giant radiating dike swarms (Campbell, 2001; Ernst and Buchan, 2001c).

Visualization of dynamic topography in the geologic record requires compilations on interregional or continent-scale geological maps. For example, the Geological Map of North America, at a scale of 1:5 million (Reed et al., 2005), reveals large lateral differences in present-day elevation of marine Cretaceous strata from <1000 m below sea-level along the Atlantic and Arctic shelf regions to over 2000 m above sea-level far from plate margins in the mountainous West (Fig. 2B). In particular, the strata associated with the Cretaceous Western Interior Seaway of western North America range in elevation from about 100- to over 2000-m, defining a topographic gradient of 0.05° (Fig. 2B). Neither plate-boundary processes, nor eustatic sea-level variations alone explain this distribution.

2.2. Interregional-scale unconformities

Interregional-scale unconformities are well documented and their origin has been debated for over a century (Dutton, 1876, 1880; Suess, 1883; Irving, 1888; Stille, 1924; Sloss et al., 1949; Belousov, 1962; Sloss, 1963, 1992; Vail et al., 1977; Miall, 2010; Şengör, 2001, 2003 and references therein; Şengör, 2016). Suess (1883) emphasized that physical processes need to be invoked to understand the significance of sequences (Şengör, 2016). In seeking global correlations, Stille (1924) plotted time charts of transgressions and regressions on intercontinental scales. In contrast, Sloss et al. (1949) pointed out that sedimentary sequences are bounded by regional unconformities that are not of the same age everywhere. They were careful to point out that rock is not equal to time; there simply is no global stratigraphy and no global episodicity in orogeny (Şengör, 2016). Sloss et al. (1949) interpreted these unconformities as times of cratonic exposure, and Burgess and Gurnis (1995) later attributed the sequences to times of continental submergence above subducting slabs, thus linking to modern concepts in dynamic topography. Wheeler (1958) constructed time-distance diagrams to visualize gaps in the sedimentary record. Sloss (1963) defined stratigraphic sequences as "rock-stratigraphic units of higher rank than group, megagroup, or supergroup, traceable over major areas of a continent and bounded by unconformities of inter-regional scope".

The most obvious discontinuity-surfaces in the geological record are: (1) true angular unconformities, which superpose horizontal strata over tilted and partly eroded strata; (2) nonconformities, which superpose sedimentary strata on deeply eroded magmatic or metamorphic basement rocks; (3) disconformities, which are erosional surfaces separating two superposed sedimentary successions (e.g., Prothero and Schwab, 2014, p. 334); Less obvious discontinuity surfaces are (4) paraconformities, which separate parallel stratal units in time, but without any obvious erosion (Dunbar and Rodgers, 1957). The associated gap in the record represents the time interval during which – relative to a surrounding region – non-deposition and/or surface uplift and erosion occurred, followed by sedimentation and/or relative subsidence.

No implicit difference about the processes leading to hiatus formation may be derived from the four unconformity-types at a single locality. They are expressions of cyclic, episodic, or singular events on different temporal and spatial scales (e.g., Miall, 2010; Pitman and Golovchenko, 1991; Christie-Blick et al., 1990). Therefore, it is essential to map the full extent of unconformities in time and space before attempting to derive their significance in the geological record (e.g., Sloss et al., 1949; Belousov, 1962; Sloss, 1963). Of greatest interest for our study are any stratal discontinuities that formed outside of plate-boundary regions, at interregional scales. Such unconformities link directly to interregional-scale uplift and subsidence that was caused by long-wavelength deformation events, not by orogeny.

2.3. Interregional-scale hiatus mapping, stratigraphic sequences, and the geological time scale

The fundamental lithostratigraphic laws of geology, known as Steno's principles, guide the interpretations of the geological record. These laws state that younger strata occur above older ones (law of superposition), were deposited horizontally (law of original horizontality), are laterally continuous (law of lateral continuity), and if a disconformity or rock body truncates or terminates another one it must be younger (principle of cross-cutting relationships) (Steno, 1669). The latter applies locally, but not necessarily on regional scales or along continental margins, where depositional facies patterns are more complex (e.g., Christie-Blick et al., 1990, p. 124–5; Şengör, 2016). Geological maps of all scales are well suited to visualize these relationships, but event-based plume-stratigraphic frameworks require examination on interregional scales.

An additional criterion, the relative age succession of strata, was established based on the principle of faunal succession (Smith, 1816) and on the biostratigraphic principle that the evolution of invertebrates is distinct and faster than the rates at which sedimentary successions form. The abundance and type of fossil species serves as the fundamental division into chronostratigraphic units, such as the Paleozoic, Mesozoic, and Cenozoic erathems (e.g., Lyell, 1833; Gradstein et al., 2004). These erathems and their subdivisions, geological systems and series, form the basis for most interregional geological maps, while even finer subdivisions (stages) are used on maps of regional to local scales. It is important to note that neither the rock nor the fossil record yields time information directly (e.g., Sloss et al., 1949; Şengör, 2016), and that true global episodicity in deposition does not exist (e.g., Şengör, 2016; Pitman and Golovchenko, 1991).

Calibration of the geological time-scale requires continuous stratigraphic sections that document the changing global fossil record across a system, series, or stage boundary (Gradstein et al., 2004) in combination with radiometric age determinations. Typically, such boundaries are found in the middle of sedimentary basins, where continuous successions are more common than at their margins. But the challenging quest for such perfect sections, i.e., the Global-Boundary-Stratotype-Section-and-Point- (GSSP) concept (golden spike, e.g., Gradstein et al., 2004; Gradstein et al., 2012; see Walsh et al., 2004), testifies that stratal successions are laterally discontinuous, incomplete, or were plate-tectonically influenced. Over 1/3 of the Phanerozoic system boundaries exposed on the continents are unconformable (Fig. 3A, Fig. DR-5A), confirming that none of the system boundaries are truly conformable on a global scale. Furthermore, hiatuses are not restricted to plate boundaries, but also occur across continental interiors (Fig. 3B, Fig. DR-5B). We assume that interregional-scale unconformable contacts (halal surfaces) on geological maps yield proxy-records of paleotopography and vertical motion of the earth's surface. Therefore, a major goal of our study is to map the duration and lateral extent of hiatuses. Ideally, temporal resolution of stage boundaries should be available on interregional geological maps, whereas presently those maps yield only system- or series-boundaries.

We define unconformable contacts on an interregional scale as those across which one or more entire system/s, or series, is/are absent. Conformable contacts are those across which no system or series is missing. From a tectonic perspective, these contacts appear arbitrarily defined, because they represent times of biological or geochemical significance (e.g., Wheeler, 1958, 1959; Sloss, 1963; Miall, 2010; Şengör, 2016). The geological map of the world and all continent-scale geological

maps have a temporal resolving-power equivalent to the durations of chronostratigraphic map units, i.e., systems, or series (tens-of-millions-of-years; Commission for the Geological Map of the World and Bouysse, 2014). Therefore, on the maps used here, time gaps (lacunas, Wheeler, 1964) in the rock record are displayed in increments corresponding to the duration of missing systems or series. They comprise timespans of non-deposition (hiatus; International Stratigraphic

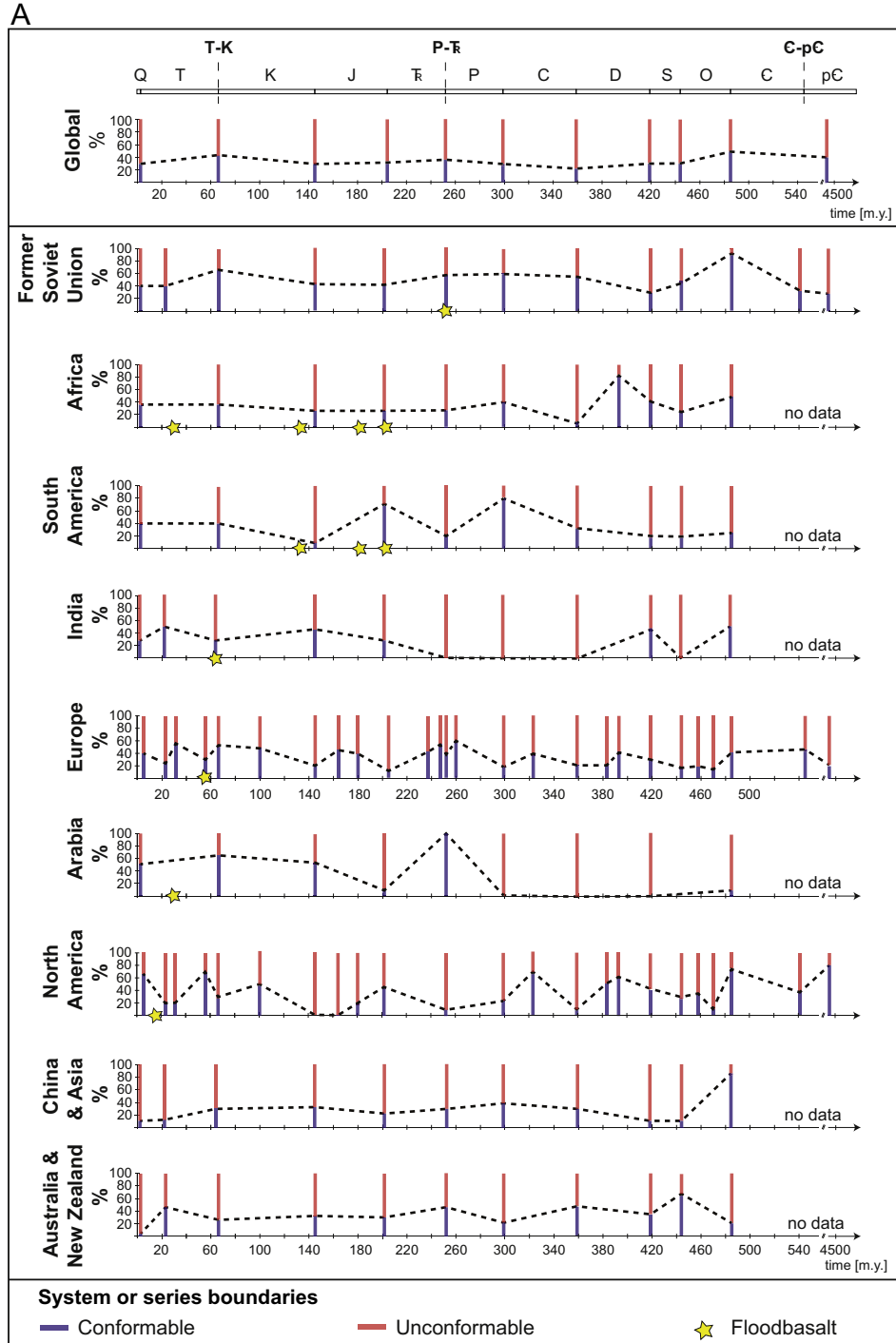


Fig. 3. Diagrams showing the proportions and the distribution of conformable versus unconformable system boundaries based on the International Geological Map of the World (1 : 5 Million) and continent-scale maps (Table DR-T1). **(A)** Phanerozoic time chart showing globally and continentally averaged percentages of conformable versus unconformable system- and series-boundaries relative to underlying system/series. Many of the Cambrian-Precambrian system boundaries are not shown, because the respective geological maps do not distinguish Late Proterozoic units. Information regarding the global and continental percentage of conformable boundaries relative to the smallest hiatuses just below each system/series boundary is shown in Fig. DR-5 (Data Repository). **(B)** Global Erathem-boundary maps showing the distribution of all Phanerozoic conformable and unconformable system/series boundaries derived from shape files of the continent-scale geological maps (Table DR-T1). Information from subsurface boundaries are not included, and the data have not been corrected for erosion.

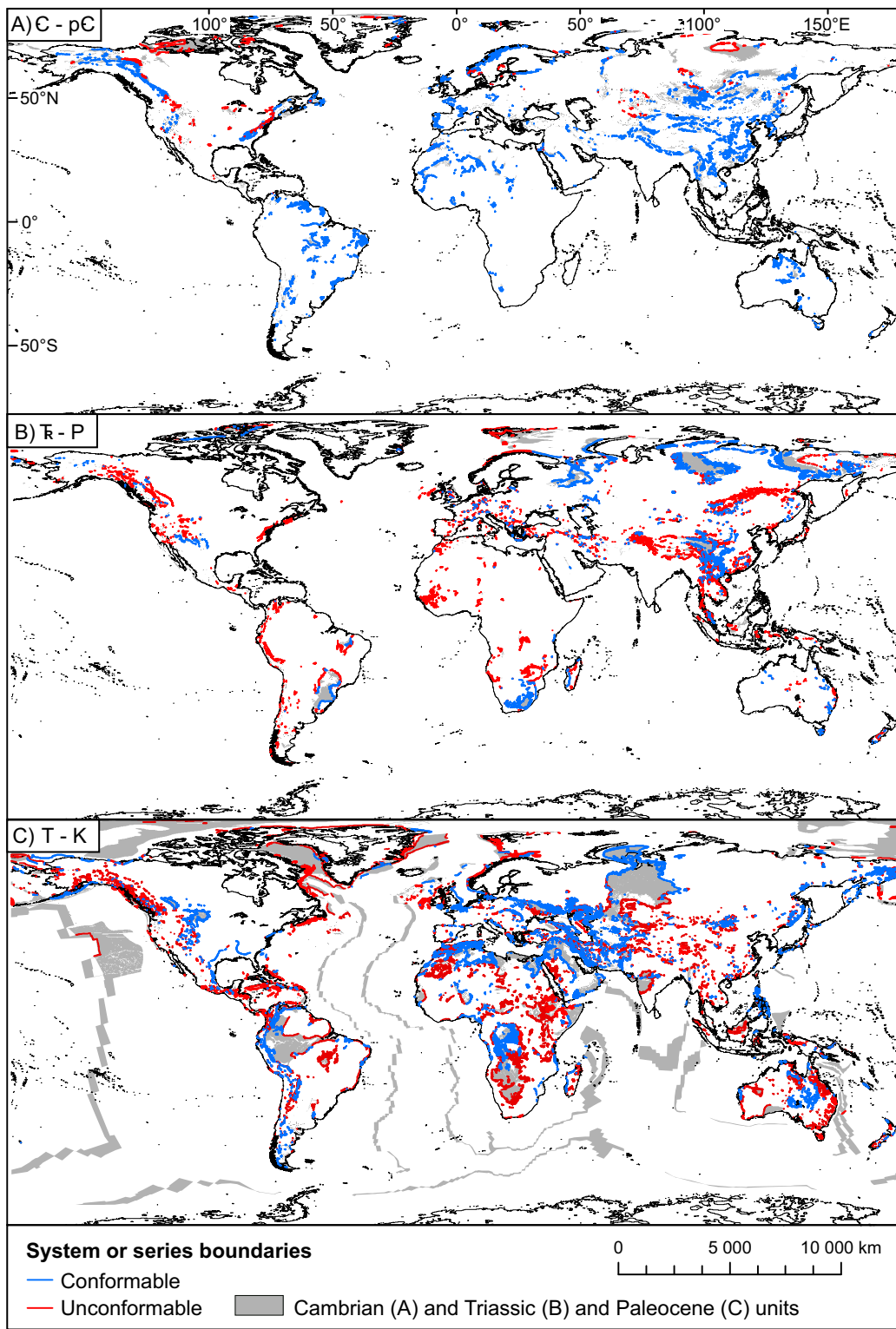


Fig. 3 (continued).

Guide, Salvador, 1994) and erosion (degradational vacuity; Wheeler, 1964). Here, we use the term hiatus, or hiatial surface, as the general term to imply missing time in a stratigraphic succession as shown on a map (see Fig. 4). The true hiatus may be larger than indicated by the missing system/s or series, because at any one location, the true age of the sedimentary units may represent but a small portion of a system or series. Therefore, currently available digital maps yield temporal

uncertainties of up to nearly 100% in cases where only one system or series is missing and the adjacent systems or series are not fully represented in the field. Interregional geological-maps at the resolution of stages would minimize the problem. Countless smaller unconformities exist (e.g., Sloss, 1963; Pitman and Golovchenko, 1991; Miall, 2010, Fig. 2.3), but these are not displayed on interregional maps. Advantageously, at low temporal-resolution only the interregionally-significant hiatuses

are visible (Figure 4B). The age of a hialtus surface may vary spatially (Sloss et al., 1949; Şengör, 2016). In this study, we show hiatus intensity as a proxy for paleotopography and their sequential changes as a proxy for vertical motion of the earth's surface (Fig. 5).

2.4. Eustatic sea-level fluctuations versus vertical motion of the earth's surface

Marine transgressions and regressions indicate fluctuations in global sea-level (eustasy) relative to local substrate, and reflect shifts in base level (e.g., Wheeler, 1964; Coe, 2002; Miller et al., 2005; Catuneanu, 2006). Scientists interpreted these signals as indicating either vertical motion of the continents (e.g., Stille, 1924) or as eustatic sea-level motions (e.g., Suess, 1883; Vail et al., 1977). However, many authors have

since pointed out that eustatic fluctuations are limited to tens-of-meters over a few millions-of-years and that change occurs on several scales, not limited to glacial eustasy (e.g., Pitman and Golovchenko, 1991; Miall, 2010; Conrad, 2013; Rowley, 2017). For example, plate tectonic processes contribute to long-term sea-level changes via thermally-controlled bathymetry over the course of the Wilson cycle (e.g., Pitman, 1978; Conrad, 2013). Marine sedimentation, compaction, isostatic responses and many other factors also contribute to eustatic sea-level, making it a truly complex signal. Rowley (2017) derived an upper limit of 100 m for the global average eustatic sea-level change. There is no process resulting in transgression or regression on a truly global scale (e.g., Pitman and Golovchenko, 1991; Moucha et al., 2008; Şengör, 2016). The level of the sea is the running sum of all processes

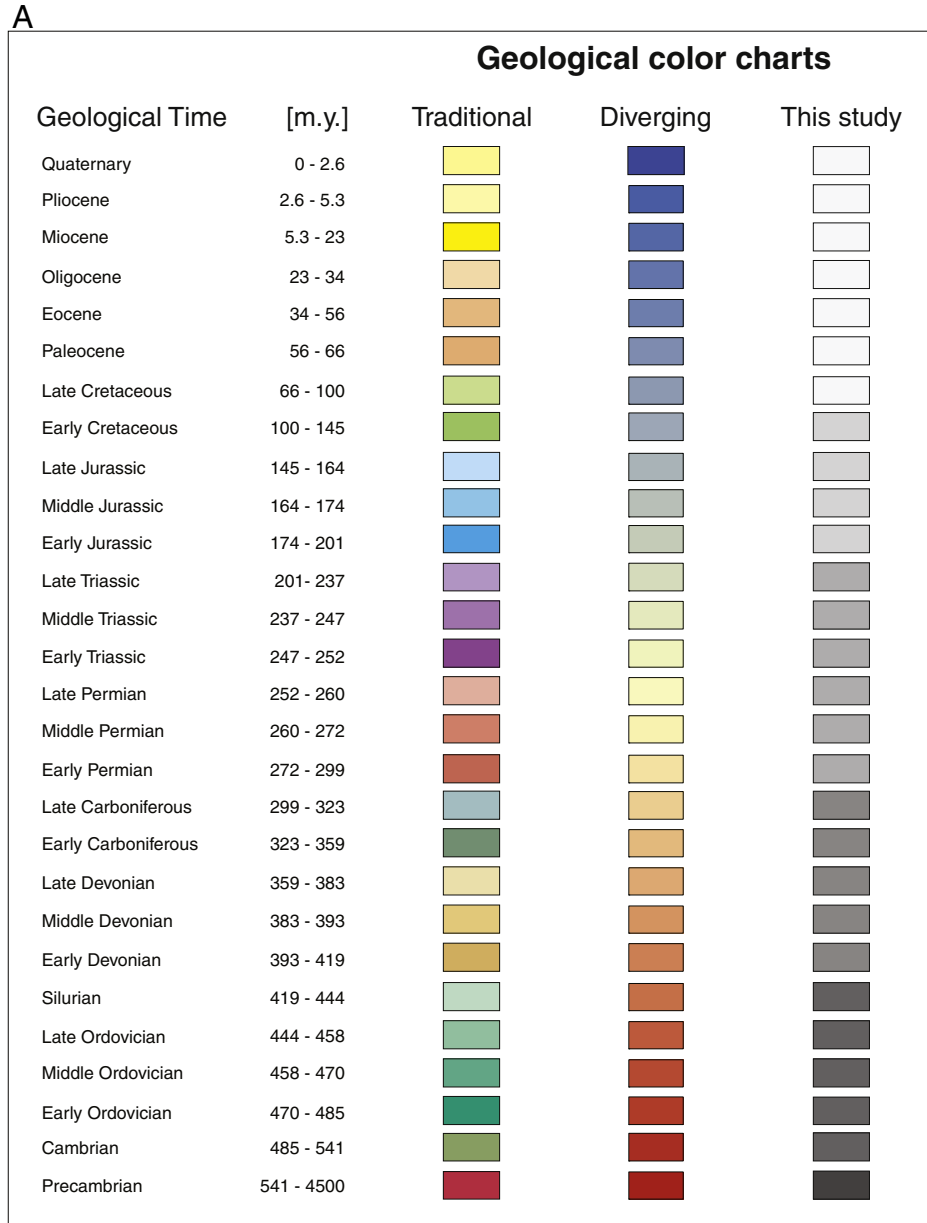


Fig. 4. Color charts and geological world maps showing the effects of various color schemes useful in visualizing interregional and global geological data. (A) Geological color charts applied to the (B) geological world maps using three different schemes: the traditional color scheme (e.g., Walker et al., 2013), a diverging red-white-blue scheme, and a nearly linear white-to-grey scheme, which we used in this study to avoid confusion with the color scheme used in Figs. 6 to 13 (Data Repository). (C) Reconstructions of the geological world map using GPLATES (Boyden et al., 2011) in the reference frame from Mathews et al. (2016) using a hybrid absolute reference frame, based on a moving hotspot model for the last 100 m.y., and a true-polar-wander corrected paleomagnetic model for 200–100 million years. Locations of major continental flood basalt provinces discussed in the text are marked in the time slice that most closely corresponds to the time of their formation. Unconformities are easily depicted based on the linear difference between two shades. Note that younger geological layers have been uncovered in older time slices to approximate the earth's surface rock record at the respective time. We note that the shape-files of digital geological maps only contain polygons representing exposed systems or series, but not their covered underground extent. This leads to uncertainties in the age of rock exposed at the surface in the past (yellow regions).

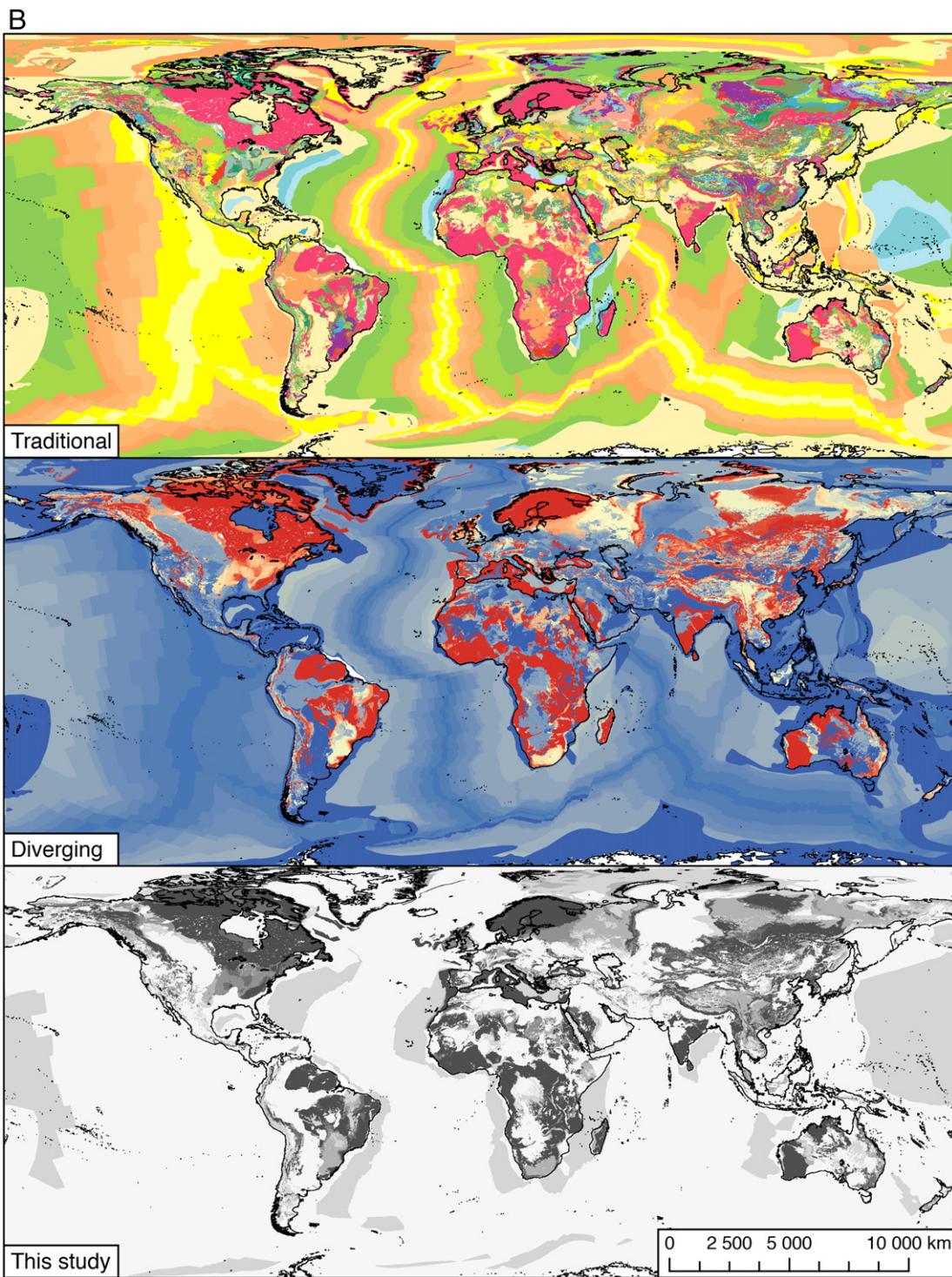


Fig. 4 (continued).

contributing to its change. Therefore, signals at high amplitude (>1 km) and interregional scale (1000 to 3000 km) are not eustatic and may be identified despite the eustatic noise.

2.5. Megasequence stratigraphic-frameworks

Unconformity-bounded successions are expressions of sedimentary deposition that result from any combination of plate- and plume-mode processes and eustatic sea-level fluctuations. Interpretation of their stratigraphic relationships requires a genetic association with one or more of these physical processes (e.g., Suess, 1883; Belousov, 1962;

Pitman and Golovchenko, 1991; Salvador, 1994, Chapter 6; Miall, 2010; Şengör, 2016). For continental margins and marine basins, stratigraphic frameworks are based on plate tectonics, eustatic sea-level fluctuations (e.g., Busby and Ingersoll, 1995; Pitman and Golovchenko, 1991), and the effects of rock compaction, lithification and isostasy (backstripping, Lemcke, 1974; Steckler et al., 1988), as well as sequence-stratigraphic principles (e.g., Vail et al., 1977; but see Catuneanu, 2006, and Şengör, 2016; Miall, 2010; and Pitman and Golovchenko, 1991). For continental interiors, stratigraphic megasequences were associated with negative dynamic topography: Burgess and Gurnis (1995) interpreted the Sloss-sequences and their

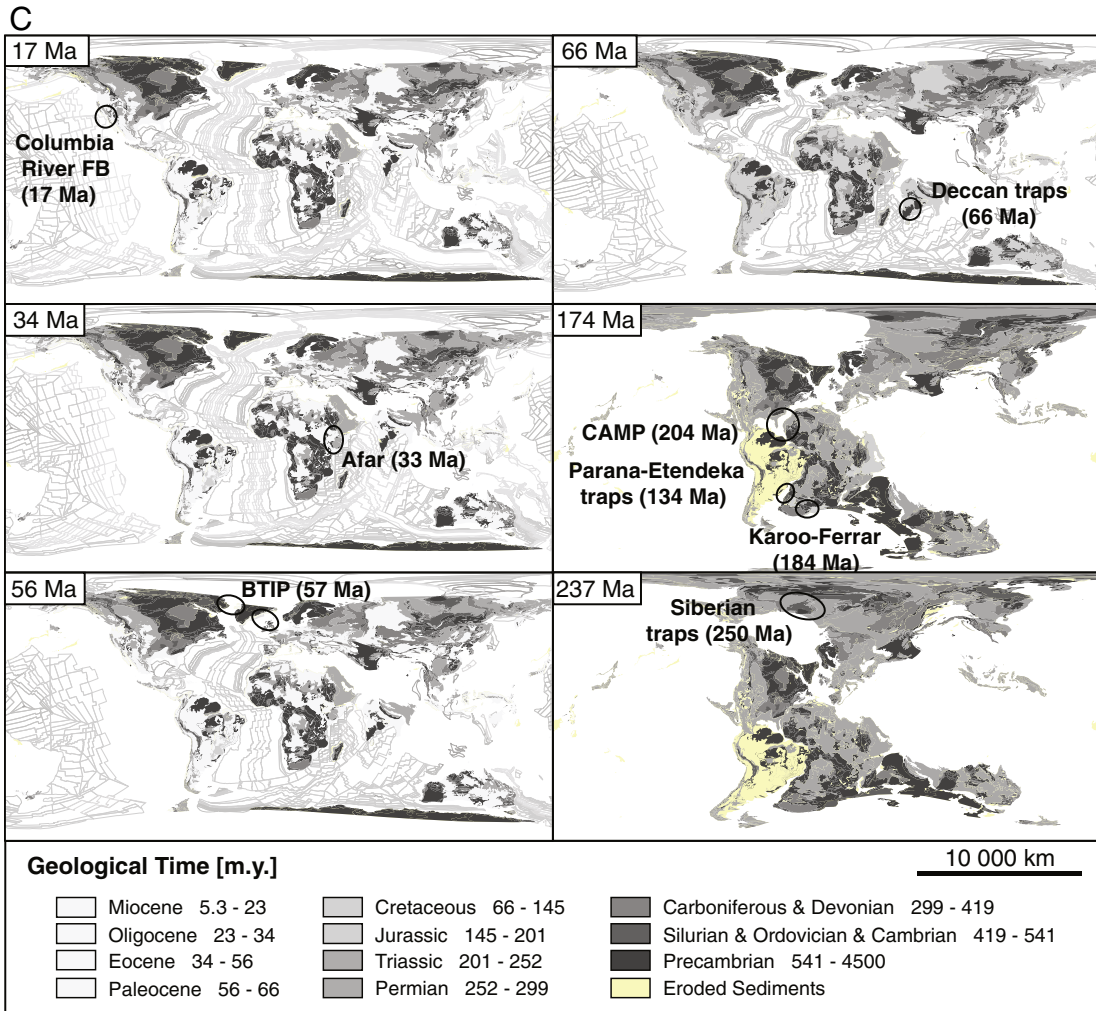


Fig. 4 (continued).

interregional unconformities on the North American craton to have formed by long-term subsidence due to subducting slabs. Here, we explore the stratigraphic consequences related to dynamically-rising mantle plumes and connect the response of the earth's surface into a plume-stratigraphic framework. We then discuss the applicability of our methodology to a Cenozoic plume-event that may be understood in a plate-tectonic context (Section 5.3) and whose flood basalts erupted on continental crust, where the geological record is likely better preserved and exposed than those related to older events.

3. Methods

3.1. An event-based stratigraphic framework for the plume mode of mantle convection

We developed testable predictions of the plume mode (Griffiths et al., 1989; Griffiths and Campbell, 1990; Campbell, 2007), i.e., those that concern the large-amplitude (>1 km) vertical response of the earth's surface on interregional scales. Mantle-plume ascent and lateral asthenospheric flow result in successive episodes of transient vertical surface-motion and systematic geomorphological and sedimentological responses that shape the geologic record (Campbell, 2001; Rainbird and Ernst, 2001; Sengör, 2001). The size of the uplifted region corresponds to the depth of the plume head below the surface. Mapping its full dimension and evolution provides a test of its depth of origin, depending on the viscosity structure of the mantle (Fig. 6A, left panel).

Dome-shaped uplift results in a large-scale radial drainage pattern (dome-flank systems, Cox, 1989), headward erosion, and deposition of sediments outside of the uplifted region (Fig. 6A). As the plume rises, the shape of the dome evolves: Its amplitude increases while its periphery shrinks (marginal region); Thus, uplift amplitude increases at the cost of its diameter and the marginal (peripheral) region of the dome undergoes transient uplift followed by subsidence. This inversion results in an unconformity-bounded sequence (Fig. 6B, left- and right-hand panels). The rate of plume ascent provides a first-order limit on the rate of knickpoint migration and headward erosion directed to the dome center. At the climax of vertical ascent, the dome collapses mechanically to form dike swarms (Ernst and Buchan, 2001a; Sengör, 2001) and narrow rifts (Burke and Dewey, 1973; Fig. 6C, transition from red to blue curve) with internally drained basins with sag ponds and lakes, after which the flood basalts erupt (Fig. 6D; Campbell and Griffiths, 1990). Only a small portion of the ascended material erupts as flood basalts, while over 90% of the excess mantle material is forced to escape laterally over large distances and at increased velocity (Campbell and Griffiths, 1990). This leads to dynamic outward-directed broadening of the uplifting surface area to over 2000 km (Campbell, 2007), resulting in an outward-shifting, transient drainage divide (Fig. 6D and E; see also Fig. 7, stages D to F). Asthenospheric flow may focus under regions of thinned lithosphere and be deflected by cratonic roots (Sleep, 1997; Ebinger and Sleep, 1998), resulting in highly asymmetric uplift- and rifting-patterns.

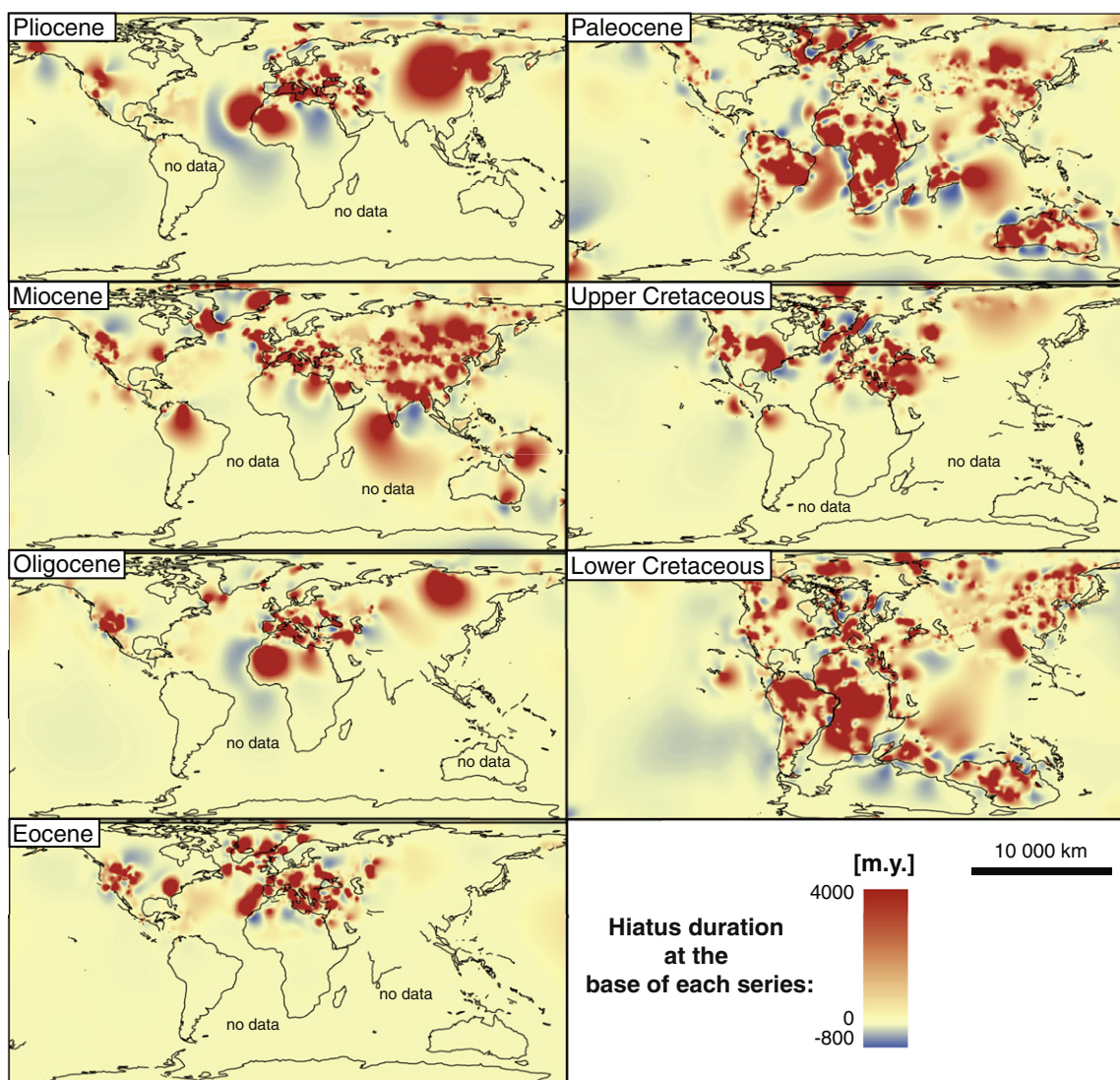


Fig. 5. Preliminary and uncorrected global hiatus maps for Cenozoic and Cretaceous series based on cubic spline interpolation. The Hiatus duration refers to the lower series boundary and indicates the size of a hiatus just prior to this boundary (Data Repository). Data base as in Fig. 3B. Reconstructions of the geological world map using GPLATES (Boyden et al., 2011) in the reference frame from Matthews et al. (2016) using a hybrid absolute reference frame, based on a moving hotspot model for the last 100 m.y., and a true-polar-wander corrected paleomagnetic model for 200–100 million years. The hiatus maps serve as a common continental reference frame to track vertical surface motion over time. In each sequential, the distribution of the hialtal areas is a proxy for paleotopography, whereas the differences between sequentials are proxies for dynamic topography.

The evolution of spatially-varying uplift and subsidence and the associated changes in erosional and depositional environments result in distinct, mappable patterns in the geological (Fig. 7, legend) and stratigraphic records (Fig. 6, right-hand panels). To illustrate the rich record of plume-related surface responses, we defined a central, marginal, and distal region in our stratigraphic and geological mapping (Figs. 6 to 9). We describe their expected characteristics below.

3.1.1. Plume center (uplifted dome, major hiatus, narrow rifting, flood basalt)

The distinct volcano-sedimentary record of dome centers has long been recognized and described for numerous large-igneous-

provinces (Ernst and Buchan, 2001a – Chapter 19; Sengör, 2001; Rainbird and Ernst, 2001; Saunders et al., 2007). The occurrence of short-lived, thick and voluminous flood-basalt units defines the dome center. Exposures of giant radial dike swarms also point to the center (e.g., Ernst and Buchan, 2001b – Chapter 12). Flood basalts unconformably cover syn-collapse strata and pre-plume basement. Prior to basalt eruption, the area is directly affected by significant uplift and erosion, formation of a dome and its collapse with extensional faulting, and internal drainage with sedimentation (Fig. 6A–E, right-hand panels – plume center). This leaves a characteristic erosional unconformity (nonconformity) in the stratigraphic record (Figs. 7 and 8).

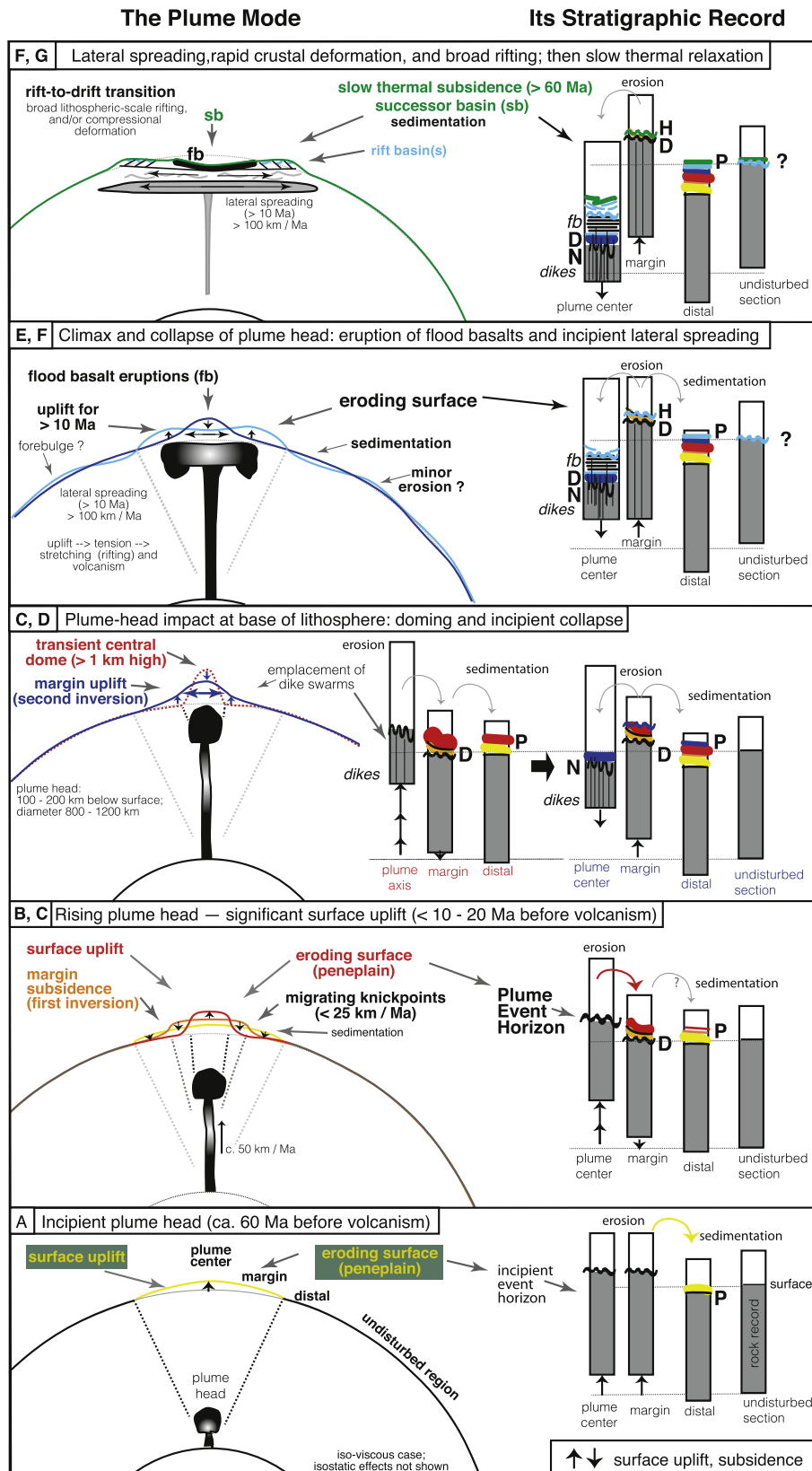


Fig. 6. Schematic diagrams showing the progressive vertical surface motion in response to a mantle-plume event (left-hand panels) as described by Griffiths and Campbell (1990) and the corresponding plume-stratigraphic record (right-hand panel) proposed in this study. The earth is drawn to scale, but the surface signal is vertically exaggerated about 1000 times. The laboratory experiment of Griffiths and Campbell (1990) simulates an isoviscous mantle. For a mantle with viscosity stratification, as indicated geodynamically (see text), the surface response may set in later, and be more complex. Panels A to G (cf. Fig. 7) show the progressive evolution of an ascending plume and its deflection of the earth's surface, with a narrowing and increase in amplitude of the affected area as the plume rises through the mantle. Related processes, such as thermal weakening and extensional thinning of the lithosphere (White and McKenzie, 1988), isostatic and eustatic responses, fracturing, diking, and details of flood basalt eruption have been omitted for clarity, but see Campbell and Griffiths (1990) or Campbell (2007). Symbols: H – Hiatus; P – paraconformity; D – disconformity; N – nonconformity.

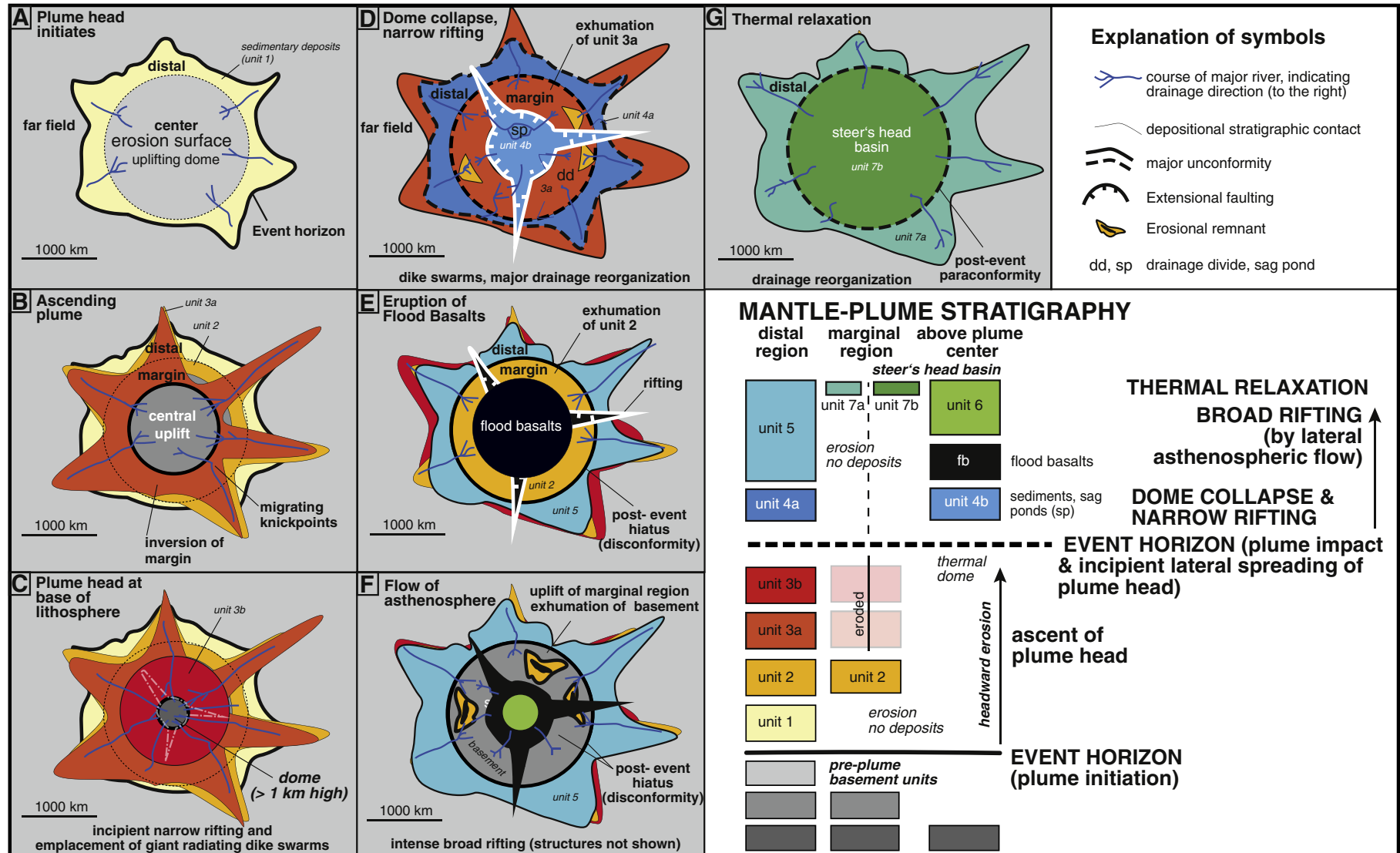


Fig. 7. Schematic sequential maps showing the hypothetical concentric and radial geological map patterns as predicted by the plume-stratigraphic model (Fig. 6), based on Campbell and Griffiths (1990) and Griffiths and Campbell (1990). (A) Progressive unroofing of older rocks in the center of the uplifting dome results in a radial drainage pattern (cf. Cox, 1989). Sediments (unit 1, yellow, cf. to legend on lower right-hand panel) accumulate in a distal position. The base of unit 1 is the plume-event horizon. (B) With plume-head ascent, the uplifting region (grey area) decreases in size but grows in elevation. Therefore, a plume margin is defined as the inward-growing dome region that experiences subsidence following incipient uplift (first inversion; Griffiths et al., 1989). Synchronously with ascent of plume head, sediments derived from the uplifting and eroding dome center are therefore deposited (units 2 and 3b) on previously exhumed pre-plume units (basement; cf. Fig. 6, model after Campbell and Griffiths, 1990). (C) Knickpoints continue to migrate upstream at $\frac{1}{2}$ the rate of plume ascent. Doming culminates prior to extensional collapse (narrow rift mode, Burke and Dewey, 1973), which leads to (D) subsidence of the central region, internal deposition (unit 4b), drainage reorganization and (E) eruption of flood basalts (black area). Depending on the precise timing between flattening of the plume-head and eruption and transport-rate of the flood basalts, the basalts either rest on plume-margin-ascent strata (e.g., unit 2, cf. hiatus D/E, Fig. 8) or on (F) uplifted and exhumed pre-plume basement units (large hiatus ABC, refer to Fig. 8), which formed in response to flattening of the plume-head. Results as outward-directed surface uplift of the plume margin. Broad and rapid lithospheric-scale deformation (e.g., broad riftting) may dominate this phase. The distal region continues to accumulate sediments (unit 5), while, say, unit 2 is re-exposed or eroded within the plume margin. The plume center acts as a sediment sink. (G) At a late stage, thermal relaxation leads to slow regional-scale subsidence and the central region fills with sediments (transgressive onlap), resulting in a steer's head successor basin (e.g., Dewey, 1982; White and McKenzie, 1988).

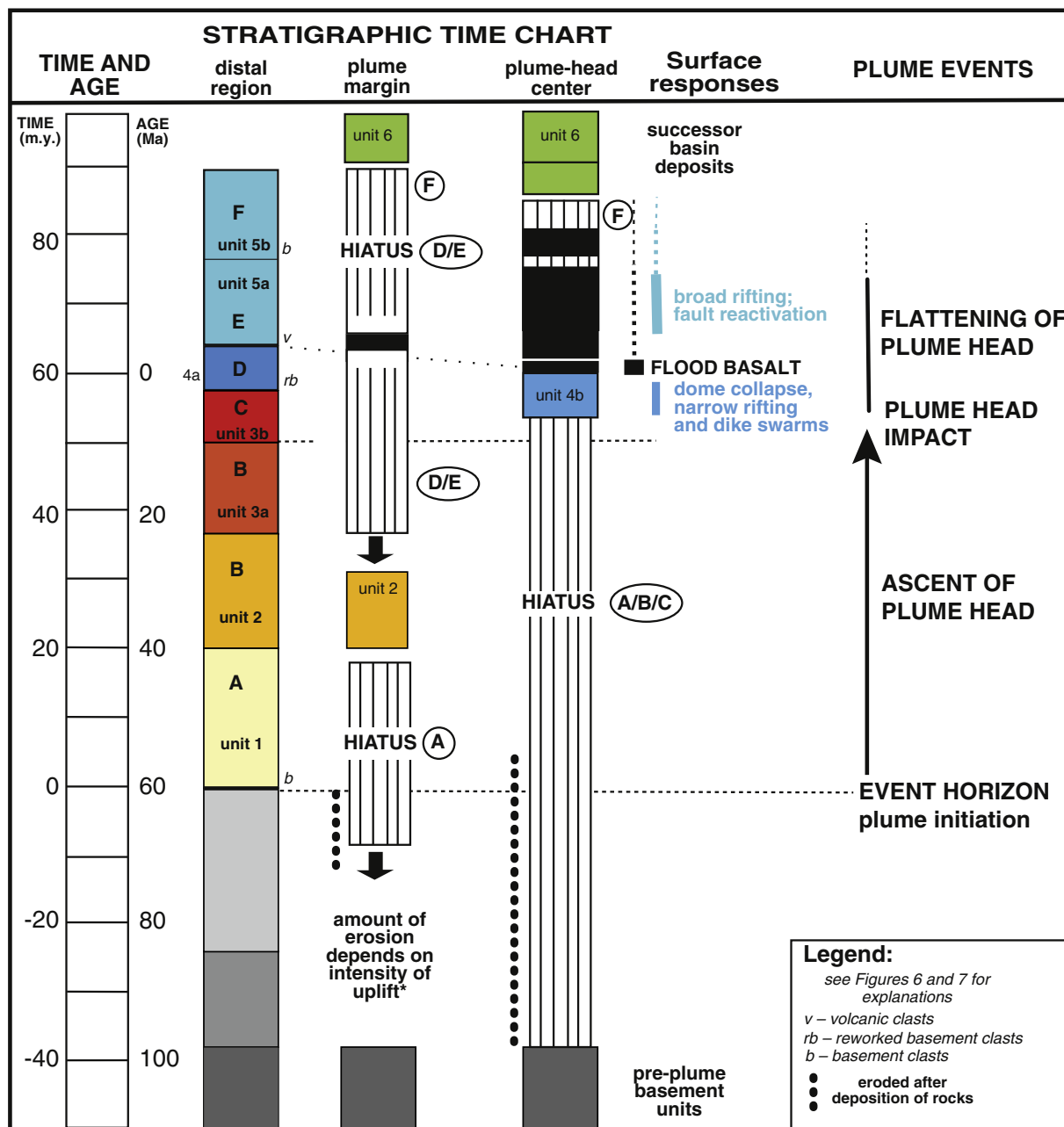


Fig. 8. Theoretical time scale and chronostratigraphic chart that would result from a plume-head event that initiated at the core-mantle boundary and ascended at a rate of c. 50 km/m.y. (Fig. 6; Colli et al., 2018—in this issue). Time scale on left is relative to mantle-plume model. Time scale on right expresses the geological age, pinned to the eruption of the flood basalts. Pre-plume initiation rock units (“basement”) are shown at arbitrarily chosen ages and depict the temporal resolution of geological series (c. 20 to 40 m.y.) typically shown on geological maps. Information on chronostratigraphic charts does not account for the thickness of a unit (refer to stratigraphic column), but best represents the formation time. Read the figure from right to left, starting with the event-center.

3.1.2. Plume margin (repeated transient uplift and subsidence, knickpoint migration, broad rifting)

The marginal area above the plume responds to plume-head ascent and flattening. It records a complex history of episodic uplift and subsidence (Fig. 6A–G) as a function of plume initiation depth, mantle viscosity structure, volume, and the rates of ascent and lateral sublithospheric flow, as well as geomorphological controls on erosion, transport and sedimentation. If at least some syn-plume-ascent strata are preserved (units 2 and 3, Fig. 8), hiatus surfaces A and D–F (Fig. 8) date plume initiation and sublithospheric lateral-flow, respectively. Here, the age of exhumed pre-eruption rocks is structurally younger than in the central region, which provides a better lower bound on the

age of plume initiation. If unit 2 strata are eroded (Fig. 8), a combined hiatus A – F testifies the whole plume event.

3.1.3. Distal region (intracontinental basin, or off-shore basin)

A distal region yields, by definition, a complete mantle-plume stratigraphic section (Fig. 6, right-hand panel). The region is not affected by plume-related uplift, nor plume-related erosion. Other processes may dominate over plume-event related deposition, such that distal deposits may occur in almost any basin setting, including plate-boundary, intracontinental, or offshore basins. True hialt surfaces within it may be of complex origin and relate to differences in sediment supply (Section 3.1.5).

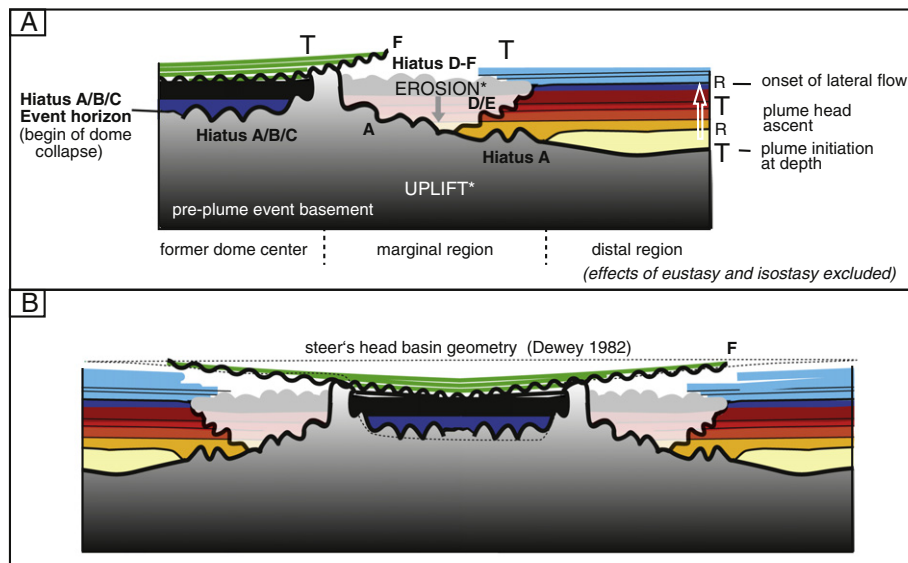


Fig. 9. Schematic sectional diagram showing stratigraphic relationships of a hypothetical plume event. The effects of other processes or eustasy are excluded. Notice in particular the two unconformities, hiatus A and D/E (Fig. 8), which are predicted for the plume margin; a double-unconformity-bounded succession forms. A characteristic transgressive-regressive-transgressive sequence is expected in the distal region. Width of area affected by erosion corresponds to the size of the plume head (hiatus A) and the characteristic of the laterally spreading plume-head (hiatus D/E). Ascent rate may be derived by reconstructing positions of transgressive onlaps.

In a continental system, for example, such a section may be characterized by fine-grained clastic successions with upwards increasing maturity of reworked basement clasts. We define the contact between unit 1 and the pre-plume basement (strata or crystalline rocks) as the event horizon that best defines the timing of plume initiation in the stratigraphic record (Fig. 8). Above it, a conformable stratigraphic section, separated by paraconformities, principally documents progressive unroofing of the dome and its margins, coeval with plume ascent. Ideally, and as long as this depositional system is not dominated by other processes, the stratigraphic units coeval with dome buildup (unit 3b, Fig. 7C, and Fig. 8) and collapse (unit 4a, Fig. 7D) document the transition from basement-derived immature clasts (unit 3b) to appearance of reworked clasts of greater maturity (unit 4a). The upper contact is defined by the first appearance of basaltic volcanic clasts (unit 5, Fig. 7E) that postdate the onset of flood-basalt eruption. A last depositional signal directly related to plume activity is the renewed appearance of basement clasts, given sufficient unroofing of the marginal region caused by lateral spreading. Eventually, sediment supply from the plume area will vanish, some 60 m.y. after initiation (Cox, 1989), as the internal successor basin collects the remaining erosion products (stage F, Fig. 7). Thermal relaxation results in a protracted re-equilibration of the landscape, which is difficult to identify in the stratigraphic record if other processes dominate. However, characteristic onlap successions are typical of this phase (steer's head basin geometry; Figs. 7G and 9; Royden et al., 1980; Dewey, 1982; White and McKenzie, 1988). We seek to visualize potential distal regions by digital mapping, bearing in mind that much sediment may have been eroded since then, or been deposited in offshore locations where eustatic effects dominate (Section 3.1.5).

3.1.4. Double unconformity-bounded sequences and event horizons

Numerous plume-related discontinuities, in particular double unconformity-bounded sequences are predicted to form in the sedimentological record across the region (Figs. 8 and 9). In the dome center, a major basal erosional nonconformity forms due to long-lived uplift, erosion, and dome collapse with internal drainage (hiatus ABC, Figs. 8 and 9); A late discontinuity forms by transgressively onlapping sedimentation onto the flood basalts as the whole region subsides due to protracted thermal cooling (hiatus F, successor basin deposits). At the active plume margin,

a lower nonconformity forms following a brief, gentle period of uplift (hiatus A, Figs. 8 and 9); The nonconformity may be eroded later due to accelerated uplift related to lateral spreading, but it is covered eventually by transgressively onlapping sedimentation during relaxation (hiatus DEF, Figs. 8 and 9). In distal regions, the sedimentary record (units 1 to 5) contains horizons corresponding to the hiatral surfaces (hiatuses A to F) of the marginal and central regions (Figs. 8 and 9). For example, hiatus ABC of the dome center is represented by units 1, 2, and 3 of the distal region. The basal discontinuity in the distal region marks the event horizon, i.e., the time of plume initiation, whereas numerous discontinuities within the units correspond to depositional modes affected by climate and eustatic fluctuations. Another event horizon (contact units 4b and 5a, Fig. 8) marks the onset of flood-basalt volcanism based on the first appearance of volcanic debris in the record; This event horizon is younger than the true onset of flood-basalt volcanism by some geomorphological response function (lag time). A final laterally diachronous disconformity marks the onset of thermal relaxation of the whole system (hiatus F, Figs. 8 and 9). In the distal region, some or all of the discontinuities may be paraconform without any erosion prior to deposition, although this depends on local transport and depositional conditions.

3.1.5. Complications owing to independent fluctuations of sea level

Whenever dynamic topography affects coastal- and offshore-regions, the uplift of the earth's surface principally contributes to eustasy in a number of ways: (1) Dome uplift instantaneously results in a regression in the central and marginal region, but in a transgression in distal regions, which are not affected by the uplift. Thus, contemporaneous strata laterally grade from regressive marginal-successions into transgressive distal-successions. (2) Deposition of plume-debris in distal regions contributes to instantaneous local regression. (3) Adjustments of eustasy to the plume-event affects sea-level, but delays of a few million years may be expected (Pitman and Golovchenko, 1991). In the distal region, these effects are superposed and difficult to untangle. During vaning-stages of plume events, the opposite applies.

The active plume-surface center experiences high-amplitude vertical movements that exceed eustatic fluctuations by far. Therefore,

separation of plume-related transgressions or regressions from those due to eustatic fluctuations is possible, because the plume-related signals are limited in time and space; i.e., they are not global (Fig. 6). However, the vertical movement in the marginal region is, per definition, much smaller and may be on the same order as eustatic fluctuations. Therefore, separation of plume-related- from eustatic-signals requires mapping and lateral correlations over the full spatial extent. Even worse, the distal region does not experience plume-related vertical surface movement, but it receives sedimentary plume-event debris that adds to eustatic fluctuations. Distal regions that are located in coastal plains or offshore settings, also are sensitive to local environment, climate, and in particular to any eustatic contributions not related to the plume event. Therefore, plume-related event horizons are difficult to identify in distal marine sections where eustatic fluctuations dominate the sedimentary record. Thus, our mapping strategy is similar to that developed to map other event-based successions and horizons (e.g., Friedrich et al., 2004). Identification of a plume-event in the stratigraphic record requires understanding of the full event-signal, by first mapping the flood basalt, then the central and marginal dome and their structures, and finally the depositionally complex distal region. In particular, to map the lateral extent of the event horizon(s), quantitative techniques such as provenance analysis will be important (e.g., Weltje and von Eynatten, 2004; Bernet and Spiegel, 2004; von Eynatten and Dunkl, 2012; Hinderer, 2012). Unconformities outside of this plume-stratigraphic program – which have their own program, framework, and dimensions – are detectable, because plume-related unconformities and disconformities are well defined in duration, rate and evolving dimension.

3.2. Plume-stratigraphic mapping of recent continental flood basalt provinces

To test the theoretical framework derived above (Section 3.1, Figs. 6–9) we applied it to selected recent and well-documented continental flood-basalt provinces (Figs. 10–12, and DR 1, 2 and 3). The color scheme for mantle-plume stratigraphy is identical to that shown in Figs. 6 to 9, but not identical to the colors shown on the geological world map (Fig. 4). Flood-basalt deposits are shown in black. On each map, warm colors mark sedimentary systems related in age to plume ascent prior to eruption of flood basalts, while blue and green colors relate to syn- and post-flood-basalt-eruption strata. The age of the flood basalt is linked to the plume-stratigraphic time chart (left-hand column in Fig. 8) and color scheme (legend in Figs. 7 and 8) to assign hypothetical plume-stratigraphic mapping units to the geological map of the respective flood-basalt province. Units 1, 2, and 3 are assigned to the next older units on the geological map and pre-plume basement rocks are converted to grey according to the temporal resolution of the map available for a region. It is difficult to identify strata related to peak-doming and collapse (stages D and E in Figs. 7 and 8) on continent-scale maps owing to limited temporal resolution (unit 4a) and to burial below the flood basalts (unit 4b). Geological units above the basalts were assigned to unit 5 (blue) or unit 6 (green) depending on their distance from the plume center (stage G, Fig. 7; e.g., Fig. 11).

Direct comparison of the color pattern of an event map with the patterns shown in stages A to G (Fig. 7) indicates the evolutionary stage of a plume-mode province. For example, the presence of large green and blue regions on the plume-stratigraphic map of the 251-Ma-old Siberian flood-basalt province (Fig. DR-X1, Data Repository) best match stage G (Fig. 7), which indicates that this plume event has entered thermal relaxation phase. Or, the 66-Ma-old Deccan flood-basalt province (Fig. 10) best matches stage F (Fig. 7), representing the incipient thermal relaxation after lateral spreading of the plume head.

3.3. Identification of plume-related unconformities on geological maps

Plume events result in a distinct temporal and spatial pattern of unconformities, which decrease in magnitude away from the center of the event (Figs. 6B and 8). Therefore, outward-directed stratigraphic mapping should help to identify elements in the marginal and distal regions beyond the well-documented events in the dome center. For example, the diagnostic major hiatal surface ABC (Fig. 8) documents erosion related to transient uplift above the rising plume. Such a surface should occur in stratigraphic sections over a regional extent of at least 1000 km, but no more than about 3000 km; This hiatus would be on order of 50 m.y., perhaps up to 100 m.y. in the center (see Fig. 6; Campbell, 2001; Bunge et al., 1998; Colli et al., 2016). The actual duration of this hiatus depends on the ages of pre-event units (Section 2.3) and on the viscosity structure of the mantle (Sections 1 and 3.1; Figs. 1 and 6 A–D). The shorter this hiatus, the faster the rise, the shallower the rising-depth of the plume, or the larger the viscosity contrast between the lower and the upper mantle. This hiatal surface ABC of the plume center correlates in time with units ABC in the distal region (Fig. 8). Identifying and mapping such hiatal surfaces in known stratigraphic sections and on geological maps may be a prime technique to quantify parameters related to past plumes. In distal regions, however, such surfaces may be masked by eustatic effects (Sections 3.1.3 and 3.1.5).

3.4. Unconformity analysis of continent-scale geological maps using linear color schemes

Geological maps are generally the most important compilations of geological work. They excel at helping the reader to identify rock units, their relative ages, their architectural relationships, and the nature of their contacts.

The color scheme shown on traditional geological maps is a result of working practice of the late 17th and early 18th centuries, optimized to identify the lithological units. It developed ever since Smith in England and Lommer, Keferstein, Goethe and Werner in Germany, defined the first assigned colors to rock units (for references see Schäfer-Weiss and Versemann, 2005). Most commonly, the color red was used for granite, whereas basalt was colored in black, limestone in blue, and sandstone often in yellow (cf. David Bressan in Scientific American on April 13th, 2014; <https://blogs.scientificamerican.com/history-of-geology/How-colors-revolutionized-geological-mapmaking/>; site visited on Oct. 23rd 2016; Oldroyd, 2013; Schäfer-Schäfer-Weiss and Versemann, 2005). However, these traditional color schemes were not designed to visualize temporal patterns of rock successions (Fig. 4A; Gradstein and Ogg, 2004; Appendix 1 in Gradstein et al., 2004).

To facilitate pattern recognition, the instant depiction of unconformable-versus-conformable contacts, and an estimation of hiatus duration, we use linear or diverging color schemes that are based on as few colors as possible (Fig. 4A). For the purpose of this paper, we use a grey spectrum for normal geological maps (e.g., Figs. 4A and 4B) to avoid confusion with the plume-stratigraphically colored event-maps shown in Figs. 6 to 13. Now, a hiatus simply corresponds to a break in the spectrum; The larger the color difference, the longer the hiatus (lacuna; Section 2.3; Fig. 4B).

3.5. Hiatus maps as proxies for paleotopography and vertical surface motion

Quantitative information about the evolution of the earth's topography is needed for comparison with dynamic-earth models. A wealth of data and their synthesis (e.g., Ziegler, 1990) is available at regional scales based on analysis of sedimentary basins (e.g., Japsen, 2018, in this issue; Kukla et al., 2018, in this issue; Vibe et al., 2018, in this issue), landscapes (e.g., Green et al., 2018, in this

issue; Guillocheau et al., 2018, in this issue), and mountains (Prenzel et al., 2018, in this issue; Sehrt et al., 2018, in this issue). Here, we explore the suitability of geological maps with their hatal surfaces as interregional reference frames. The system hiatuses, which serve as proxies for paleotopography – and their sequential changes, which serve as proxies for vertical surface motion –, will need to be calibrated using information about uplift and subsidence from adjacent mountains or basins, such as thermochronology and subsurface data. Examination of the distribution of hatal surfaces on Figs. 3A, 4B, and 5 confirms that a sufficient number of hatal surfaces are of interregional size. However, these values constitute minima and must be corrected for concealed or eroded portions.

We plotted the duration of hiatuses in millions-of-years for each system- or series-boundary (Fig. 5). The hiatus duration at the lower boundary of a given system or series is read directly from the geological map, based on the geological time scale (e.g., Gradstein et al., 2012; Walker et al., 2013). For conformable contact segments, the hiatus duration is 0 m.y., whereas unconformable contacts yield a hiatus duration incrementally greater, defined by the chronostratigraphic resolution on a given map. The true values are larger if mapped successions do not represent the whole system or series. We then contoured the hiatus points using cubic spline smoothing (Fig. 5, Data Repository) to visualize the possible areal extent of hatal surfaces. Negative hiatus values on Fig. 5, which are artifacts of the interpolation, do not exist, but serve as a preliminary proxy for the approximate hatal limits, i.e. marking regions of sedimentation or subsidence. To correct the raw hiatus data for any uplift and erosion that occurred in earlier time intervals, we subtracted the hiatus values of all older hiatuses successively from the next-younger ones (Data Repository). The true areal extent of concealed and eroded hatal surfaces was not yet incorporated in the automated mapping and interpolation procedure.

To visualize the hiatuses in context of their plate neighbors at the time of plume-impact events (Fig. 4C), we rotated the present-day hiatus map back in time according to the recent rotation model of Müller et al. (2016). We used the open-source plate reconstruction software GPlates (Boyden et al., 2011) and the compilation of Ernst and Buchan (2001b) regarding plume-event age and position.

4. Results

4.1. Interregional hatal surfaces

Interregional hatal surfaces occur on all continents and throughout Phanerozoic time (Figs. 3 and 4B, Fig. DR-5). Globally, none of the system or series boundaries are either all conformable or all nonconformable (Fig. 3A). However, large variations in this ratio occur within continents or regions over time (Fig. 3A). On a global average, all Phanerozoic system and series boundaries yield an approximately constant ratio between conformable (c. 80%) and unconformable (c. 20%) boundary segments for the interval directly preceding a particular time boundary (Fig. 3A; Fig. DR-5B).

Preliminary hiatus maps for Cretaceous to Cenozoic time are shown in Fig. 5. Numerous hatal surfaces in Fig. 5 are on the order of millions of square kilometers, for example those across Africa at the base of the Lower Cretaceous and the Eocene. Large hatal surfaces vary spatially and change over time. A large Upper Cretaceous hatal-surface centered over the North Atlantic, changes into a smaller hatal in the center with outwards-shifting large hiatuses around it at the base of the Paleocene and Eocene series, respectively. In western North America, a plate-margin-parallel hatal surface appears at the base of the Paleocene, but at the base of the Eocene, an E-W-oriented interregional hatal-surface forms. At the base of the Oligocene, the hatal surface is round with a diameter of c.

2000 km, whereas at the Miocene base it splits in a southern and northern portion. The latter also exists at the base of the Pliocene. These examples show that interregional hatal surfaces change on million-to-tens-of-million-year scales. Such rapid changes are inconsistent with the plate mode, but expected by the plume mode (Section 1).

4.2. Plume-stratigraphic framework mapping

Results of the plume-stratigraphic-framework mapping are shown for the Deccan flood basalts in India (Fig. 10), the Etendeka-Parana flood-basalt province of South America and Africa, (Fig. 11, and Figs. DR-3 and DR-4), and the Columbia River flood-basalt province of North America (Fig. 12). Maps of the Siberian flood basalts, and of the North Atlantic magmatic province II of northern Europe are shown in the Data Repository (Figs. DR-1, DR-2). Figs. 10 to 12 (and DR-1 to DR-4) illustrate the context and scale over which individual geological, petrological, tectonic, geomorphological, and sedimentological features have been affected by the plume event. The main parameters are summarized in Table 1 and discussed in Section 5 below.

5. Interpretation of plume-stratigraphic maps

Below, we briefly interpret the main findings of the plume-stratigraphic mapping, bearing in mind that the published maps were not compiled with our purpose in mind. Our results and analysis are therefore preliminary and we focus on the potential to identify the spatial extent and to visualize spatial and temporal patterns related to a plume event.

5.1. Deccan-traps plume-head event

The Deccan traps (black) and their tectonic setting have been described previously (e.g., Muckherjee et al., 2017; Mahoney, 1988). The flood-basalt province and the junction of the three rift-arms define the center of plume-head impact below the lithosphere (Fig. 10). Oceanic rifting followed flood-basalt eruption and truncated the western portion of the area affected by the plume head (Sahu et al., 2013; Todal and Edholm, 1998). This also explains the asymmetric shape of the interregional-scale drainage network, whereby the drainage divide separates the narrow Western Ghats from the Deccan plateau (Cox, 1989; Sahu et al., 2013; Richards et al., 2016). This radial drainage pattern is characteristic of either stage E or stage F (Fig. 7), but the presence of both Cenozoic rift-basin sedimentary deposits overlying the basalts and the high Deccan plateau, indicate that stage F may have been reached.

Most of the Deccan traps rest unconformably on Proterozoic and Archean basement, which is exposed across most of the subcontinent. The unconformity corresponds to hiatuses ABC and ADE (Fig. 8, Table 1). Both, the Lower Cretaceous depositional pulse in the Cauvery, Krishna, and Godavari basins and the interregional-scale hatal surface at the base of the Lower Cretaceous (Fig. 5) indicate that plume-related uplift and erosion may have started around that time, whereas dome uplift with accelerated erosion and deposition occurred during the Upper Cretaceous (see Fig. 8 in Sahu et al., 2013). In the vicinity of the Narmada-Son rift, the flood basalts rest on Triassic-Cretaceous strata, the youngest deposits of which may correspond to unit 4b (Fig. 8). The distal sedimentary record is mostly buried underneath the Himalayan foreland basin or was transported to offshore depositional centers, such as the Krishna-Godavari basin (e.g., Sahu et al., 2013). This is consistent with findings by Sinha et al. (2009) that Archean-basement-derived alluvial deposits occur in the middle of the Himalayan foreland basin, indicating that sediments are shed northwards from the craton to the foreland basin. Thus plume-related dynamic topography with uplift

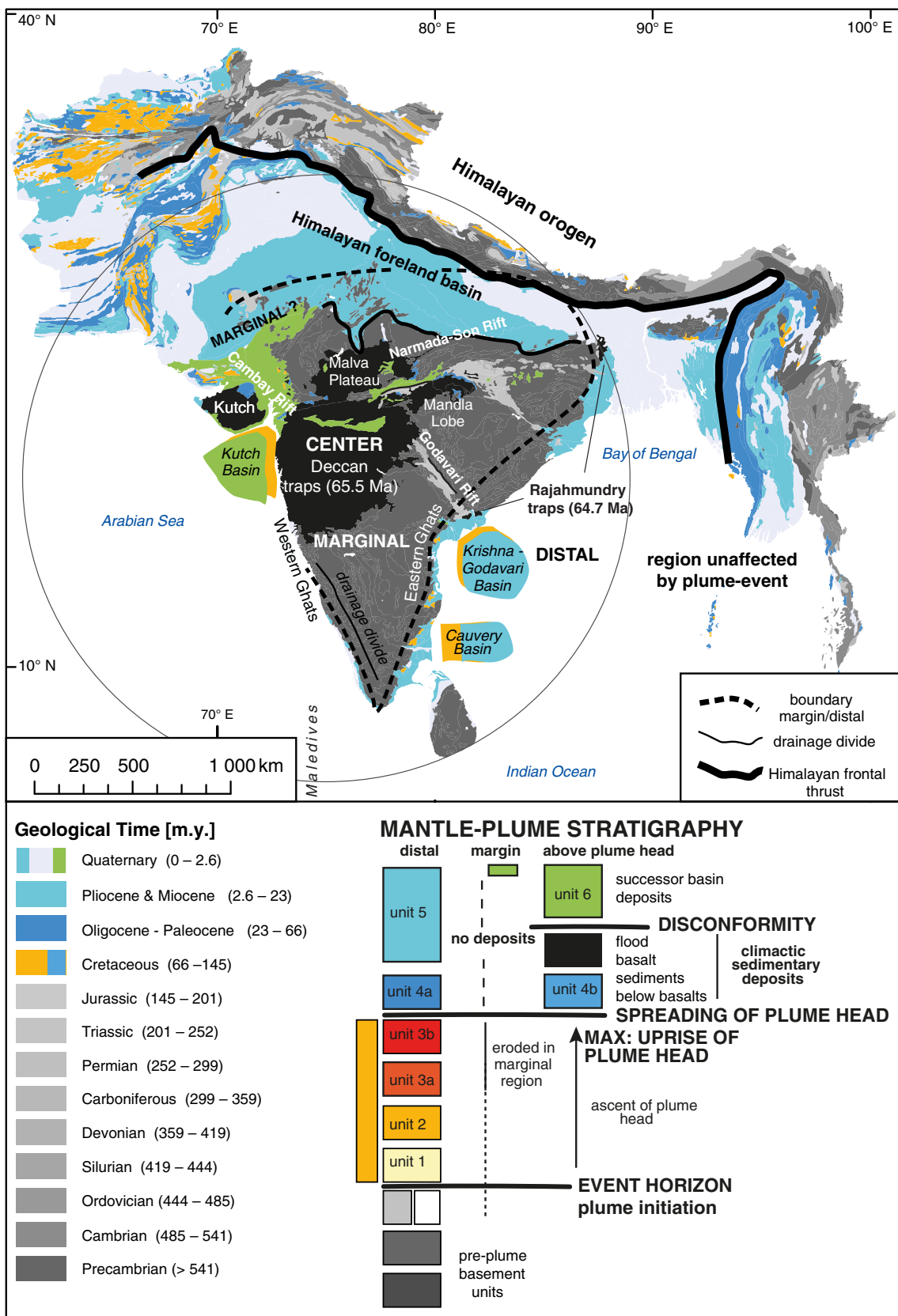


Fig. 10. Preliminary plume-stratigraphic framework of India based on the geological map of India and surrounding regions (Dasgupta et al., 1993; Wandrey and Law 1999) showing the preliminary plume-stratigraphic facies distribution (Figs. 7 and 8) related to the 66–65 Ma Deccan flood basalt province (e.g., Baksi, 1994; Courtillot et al., 1999).

and erosion continues to modify and influence the behavior of the Himalayan foreland basin and the orogen itself. Dynamic

lithospheric models of the Himalayan foreland-basin would need to consider these effects.

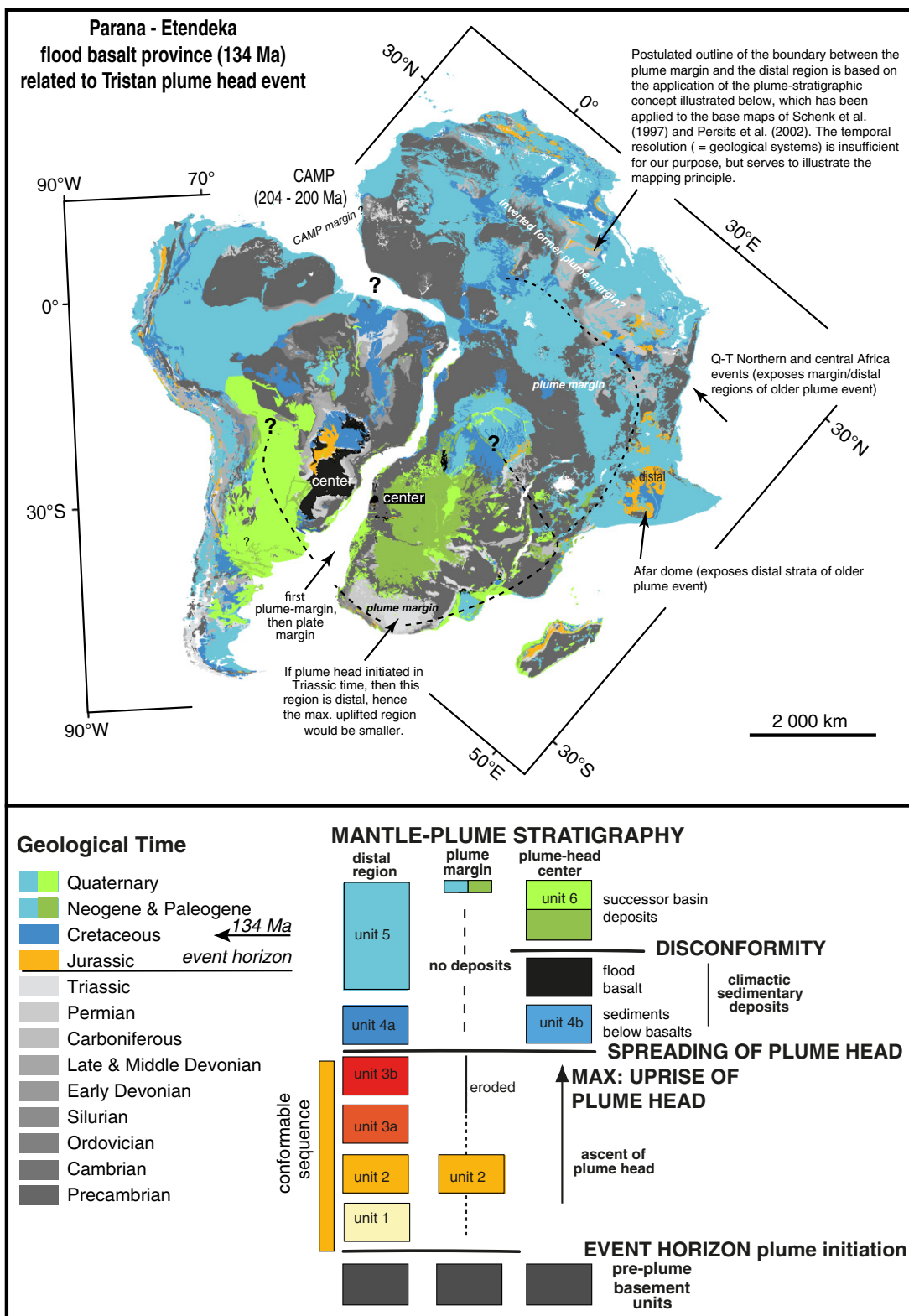


Fig. 11. Preliminary plume-stratigraphic framework for the 134-Ma-Paraná-Etendeka flood basalt province based on the geological maps of South America and Africa in their relative positions prior to breakup. Both plates were also affected by the Central Atlantic Magmatic Province (CAMP) at 204–200 Ma, the 183–180 Ma Karoo flood-basalt province, and that Africa experienced recent magmatic activity along the East African Rift System (EARS).

5.2. Paraná-Etendeka plume-head event (South America and Africa)

The Paraná-Etendeka flood-basalt eruption preceded rifting of the South-Atlantic ocean at this location by <20 m.y. (Peate, 1997; Heine et al., 2013). It is one of several plume events to have affected Africa and South America prior to continental break-up (Burke and Dewey, 1973; Fig. 19 in Sengör 2001). Opening of the South-Atlantic Ocean moved South America farther from the plume source, whereas the African plate has been stationary since at least Miocene time and continues to experience episodic dynamic uplift (e.g., Thiessen et al., 1979; Al-Hajri et al., 2009). Africa is characterized by numerous young basins and domes (e.g., Krenkel, 1922; see plate II and Fig. 4 in Krenkel, 1925, 1926; Burke and Gunnell, 2008), whereas South America experienced only two older plume-related events at 204–200 Ma (CAMP) and at c. 134–132 Ma (Paraná-Etendeka; Ernst and Buchan, 2001b; Courtillot and Renne, 2003).

Our plume-stratigraphic map for the Paraná-Etendeka event reveals additional differences between Africa and South America in the character of hiatal surfaces and the age of pre-plume basement rocks (Fig. 11). The Paraná flood-basalts (South America) are exposed and rest on a Devonian to Jurassic succession, which implies limited dome uplift prior to basalt eruption compared with the African side (Fig. 11). The Etendeka basalts (SW Africa), which are mostly covered by younger strata, have been deposited on Proterozoic rocks, defining a significant hiatus ABC (Fig. 8, Table 1). This hiatus extends across most of south-central Africa and farther north. Therefore, evidence for significant interregional-scale uplift is preserved on the African side, implying proximity to the plume-head center (Fig. 11). In South America, Paleogene to Neogene sediments eroded from the Andes might dominate the sediment volume, whereas in Africa large post-plume-event sedimentary deposits formed despite the absence of comparable mountain belts. Any sign of thermal relaxation derived from successor-basin sediments in Africa is superposed by younger plume events that resulted in renewed uplift, erosion and sedimentation (Fig. 11). For example, strata of Cretaceous age may represent the successor-basin facies related to the Karoo and time-equivalent plume events, or they may represent the distal deposits related to much younger plume events (e.g., Fig. DR-3, Data Repository). Mapping of these events is only possible after volcanic centers have been identified, and in conjunction with numerical models of mantle dynamics.

5.3. The Columbia River flood-basalt and the Yellowstone plume-event: plume-plate interaction in western North America

The Columbia River flood-basalt erupted c. 17–16 m.y. ago under northern Nevada and southern Oregon (Fig. 12; Reidel et al., 2013). Since then, the North American plate continued its southwesterly motion at a rate of 30 km/m.y., producing the Snake-River plain and Yellowstone caldera as surface expressions of the plume tail (Pierce and Morgan, 1992; Reidel et al., 2013). The plume head and its collapse are expressed by numerous geological and petrological features (Pierce and Morgan, 1992; Reidel et al., 2013; Camp, 2013, p. 181ff): At the same time as flood basalts erupted across southeastern Oregon and rhyolitic volcanism occurred at the western edge of the Snake River plain, extension initiated in the northernmost Basin-and-Range Province (Reidel et al., 2013). Camp (2013) summarized evidence for uplift prior to (e.g., Hooper et al., 2007), and during flood-basalt eruption in Oregon. Uplift set in rapidly and proceeded in a northerly direction (Camp and Ross, 2004). Pierce et al. (2002) document a north-south-oriented dome, extending for over 1000 km across the northern Nevada rift-system to the Chief Joseph and Monument dike-swarms in the north. In our plume-stratigraphic framework, these features are characteristic for the central region (Fig. 6). Further evidence for widespread uplift was reported by Flowers et al. (2008), who point out that uplift of the Colorado Plateau region had occurred by Early Eocene time, and was followed by substantial uplift around 25–20 Ma. A detailed

accounting of all observations consistent with this frame is beyond our scope. All of it points to a spectacular, because recent, example of the complex consequences that occur when the plume-mode and the plate-mode interact above an active plate-margin, which formed on heterogeneous and heterogeneously-behaving lithosphere.

The abrupt period of uplift in the northern portion at the time of basaltic volcanism and dike injections, but limited extension, corresponds to the collapsing dome (Fig. 6C and D; stages C to D in Fig. 7). The present-day limits of the central region are highly asymmetric on the Geologic Map of North America (Reed et al. 2005; Fig. 12A), because the region was affected by significant younger deformation (dextral strike-slip and east-west-extension, e.g., McQuarrie and Wernicke, 2005). We marked the region above the plume head at the time of its impact with the lithosphere at 17 Ma (Fig. 12B, inset). We account for later deformation and plate motion (Atwater, 1970), by marking the approximate locations of the plume head underneath North America at 32 Ma (Oligocene) and 46 Ma (Eocene; Engebretson et al., 1985, Fig. 3A to D).

To determine the entire surface area affected by the Columbia River plume-head event, we applied the plume-stratigraphic framework and mapped the central, marginal and distal regions. Given the resolution limits on the Geologic Map of North America (Reed et al., 2005; Fig. 12), the sedimentary strata coeval with and following flood-basalt eruption (units 4a and 4b, Figs. 7 and 8) are assigned to the Miocene (blue colors in Fig. 12). We initially assumed a plume-ascent velocity of 50 km/m.y. (Colli et al., 2018, in this issue). In this case, the expected duration of plume ascent from the core-mantle boundary to the base of the lithosphere is about 60 m.y., which places our initial guess of the event horizon's age at c. 77 Ma (Late Cretaceous time, Fig. 12A), i.e., 60 m.y. prior to the 17-Ma-flood basalt eruption. Therefore, sedimentary successions of upper Cretaceous to mid-Miocene age were mapped as distal, implying late Cretaceous plateau uplift as expression of plume-head ascent, but the size of the marginal-region affected by dynamic topography would be restricted to the Basin-and-Range Province, excluding the Colorado Plateau. In this case, a mechanism unrelated to the plume mode would have to account for plateau uplift. A better fit is illustrated in Fig. 12B, where the marginal region is larger and well-defined in the Northwest, North, and East. In this case, the absence of Paleocene deposits on the plateau would be consistent with the two-phase surface uplift of the Colorado Plateau postulated by Flowers et al. (2008) as part of the marginal region above the ascending plume-head. For an even faster ascent velocity (100 km/m.y.), a younger initiation time and event horizon (47 Ma; Eocene, Fig. 12C) applies, which is also consistent with observations. The true answer is presently unknown, but iterative mapping, data assimilation, and modeling may yield robust answers in the future.

The plume-margin overlapped with the active plate-margin and the northern and central Basin-and-Range Province. In the Oligocene, the northern Basin-and-Range Province experienced intense explosive volcanism (Lipman et al., 1971; ignimbrite flareup, Coney, 1978; Best et al., 2013). Mid-Miocene topography-defining extension postdates the ignimbrite flare-up, but may have formed as a consequence of broad rifting related to lateral spreading of the plume head in a southeasterly direction, consistent with observations and trigger mechanisms recently summarized and suggested by Camp et al. (2015). Reidel et al. (2013) pointed out that many features (subsidence, Basin-and-Range extension in the north at 17–16 Ma, basaltic volcanism and rhyolitic volcanism at the edge of the Snake River Plain) are consistent with lateral spreading of the plume head. Our mapping indicates that this process also may have led to extension in central Nevada and western Utah by mid-Miocene time (e.g., Stockli, 2000), perhaps including activation of the Wasatch fault system at c. 12 Ma (e.g., Friedrich et al., 2003). This yields a rate of propagation of extension of about 100 km/m.y., which is consistent with predictions from mantle dynamics (Colli et al., 2018, in this issue). Younger reactivation of faulting in the Eastern California Shear Zone and the Basin-and-Range Province (e.g., Colgan et al., 2004) is probably related to ongoing plate-mode deformation (e.g., Bennett et al., 2003).

In summary, our plume-stratigraphic mapping indicates that the ascending Columbia River plume-head may have interacted with the convergent North-American plate-margin well before eruption of flood basalts at 17 Ma. The region affected by surface uplift prior to eruption included the active plate margin, the northern and central Basin-and-Range Province, and probably the Colorado Plateau, equivalent to a radius of about 1200 km. A second episode of uplift affected the same region in mid-Miocene time owing to plume-head spreading (asthenospheric flow). This process triggered the main phase of Basin-and-Range

extension between 17 and 12 Ma and led to significant uplift of the Colorado Plateau (second inversion, Fig. 6D and E). The distal sedimentary record of this event may be found in the Eocene-Oligocene stratigraphic successions of northeastern Utah and Wyoming. The more severely uplifted and eroded southern margin of the Colorado Plateau, the Mogollon rim, may have felt the first dynamic-topography effects above the rising plume head. Prior to the Paleocene, the active margin of the North American plate appears to only have been affected by the plate mode, but by Eocene time, the rising Columbia River plume-head

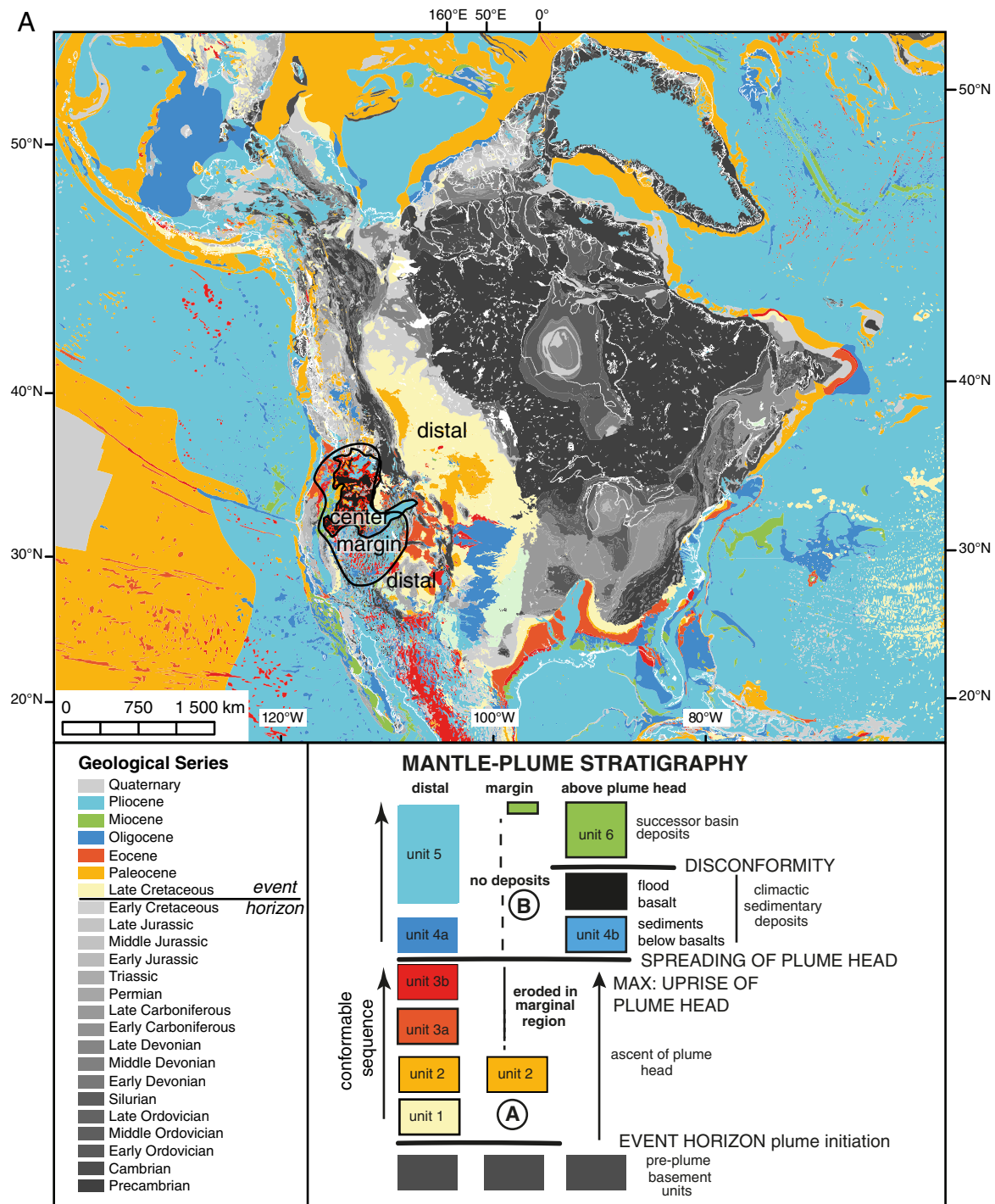


Fig. 12. Preliminary plume-stratigraphic framework for the Columbia-River plume-head event of North America, based on the Geological Map of North America and surrounding regions (Reed et al., 2005). We assumed three different plume initiation times, which are the base of the (A) Late Cretaceous system, (B) the Paleocene, (C) and the Eocene. Notice that areal extent and locations of distal regions and plume margin vary depending on which time frame is used as discussed in the text. (D) A randomness test for the plume-stratigraphic framework. Y – Yellowstone. CP – Colorado Plateau.

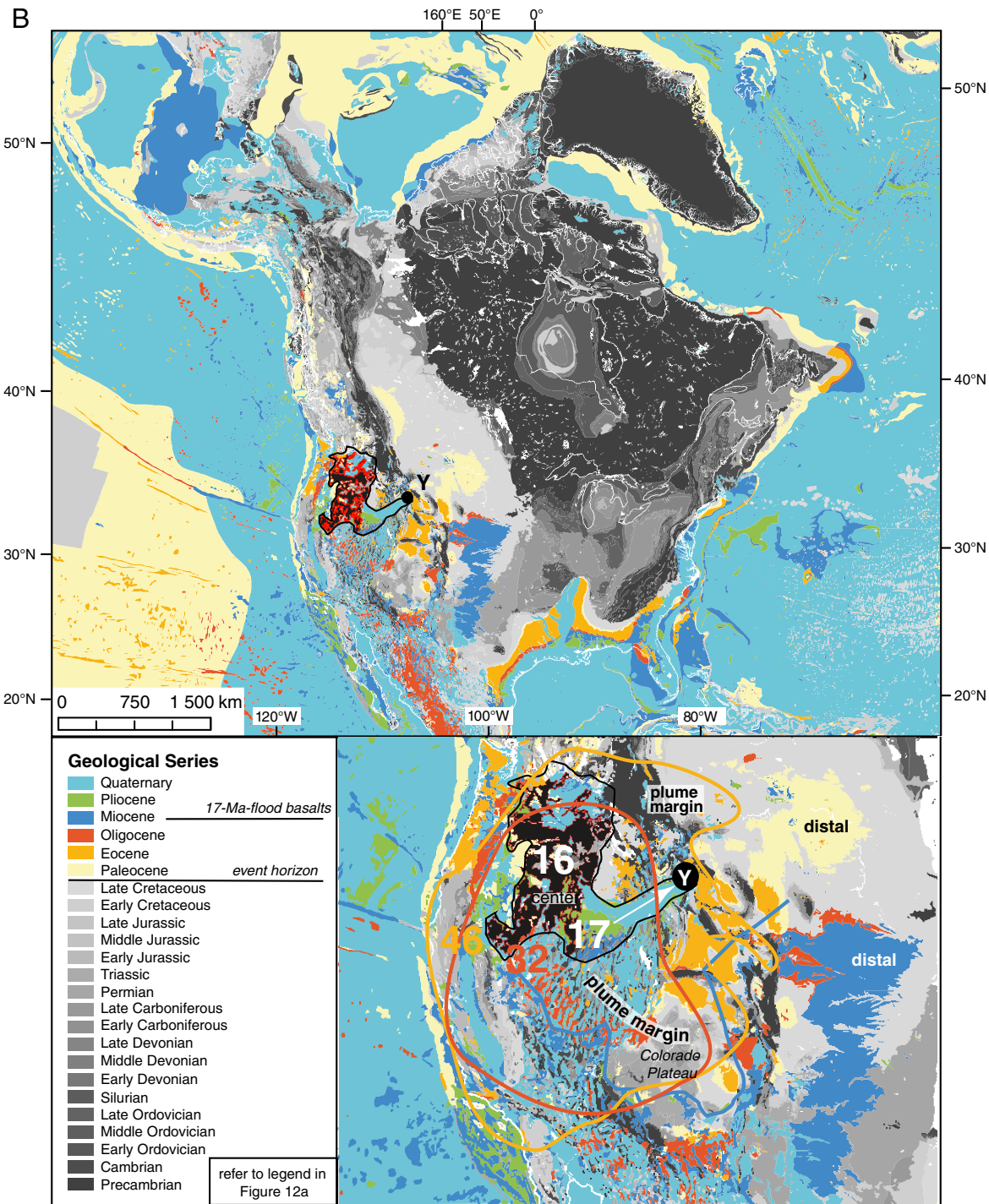


Fig. 12 (continued).

provided a dynamic setting that affected the North American lithosphere in direct and indirect ways. To understand this complex evolution, the plate tectonic framework must be complemented by a plume-stratigraphic framework. A wealth of geological data may be reinterpreted in the light of the plume model. The works of Pierce and Morgan (1992), Camp (1995), Wernicke (1981, 2011), Flowers et al. (2008), Galloway et al. (2011), Henry et al. (2012), Karlstrom et al. (2012), Best et al. (2013), Camp et al. (2015), Kincaid et al. (2013), and many others constitute significant individual pieces of this puzzle.

At the time of initiation of the Yellowstone plume head at the core-mantle boundary, the western edge of the North-American plate must have been located above it, or been in its vicinity. Thus, the initial

dome-shaped uplift (Fig. 6A) affected both the subducting Farallon plate (Engebretson et al., 1985, Fig. 3C), and the western edge of the overriding continent (Fig. 13). As the North-American plate moved at 30 km/m.y. (Pierce and Morgan, 1992; Camp, 2013) towards and over the rising plume-head (max. 100 km/m.y.) in a southwesterly direction, the size of the uplifting surface area increased as the plate moved fully over the plume head, but it decreased with rising plume-head (Fig. 6B; Griffiths and Campbell, 1990). The answer depends on the ratio between plate motion (c. 30 km/m.y.) and plume-head ascent (c. 25 to 50 km/m.y., Colli et al., 2016, 2018, in this issue). Geological observations will place constraints on this ratio once the entire signal of surface uplift will have been identified (Figs. 6B and 13). The rising plume-head

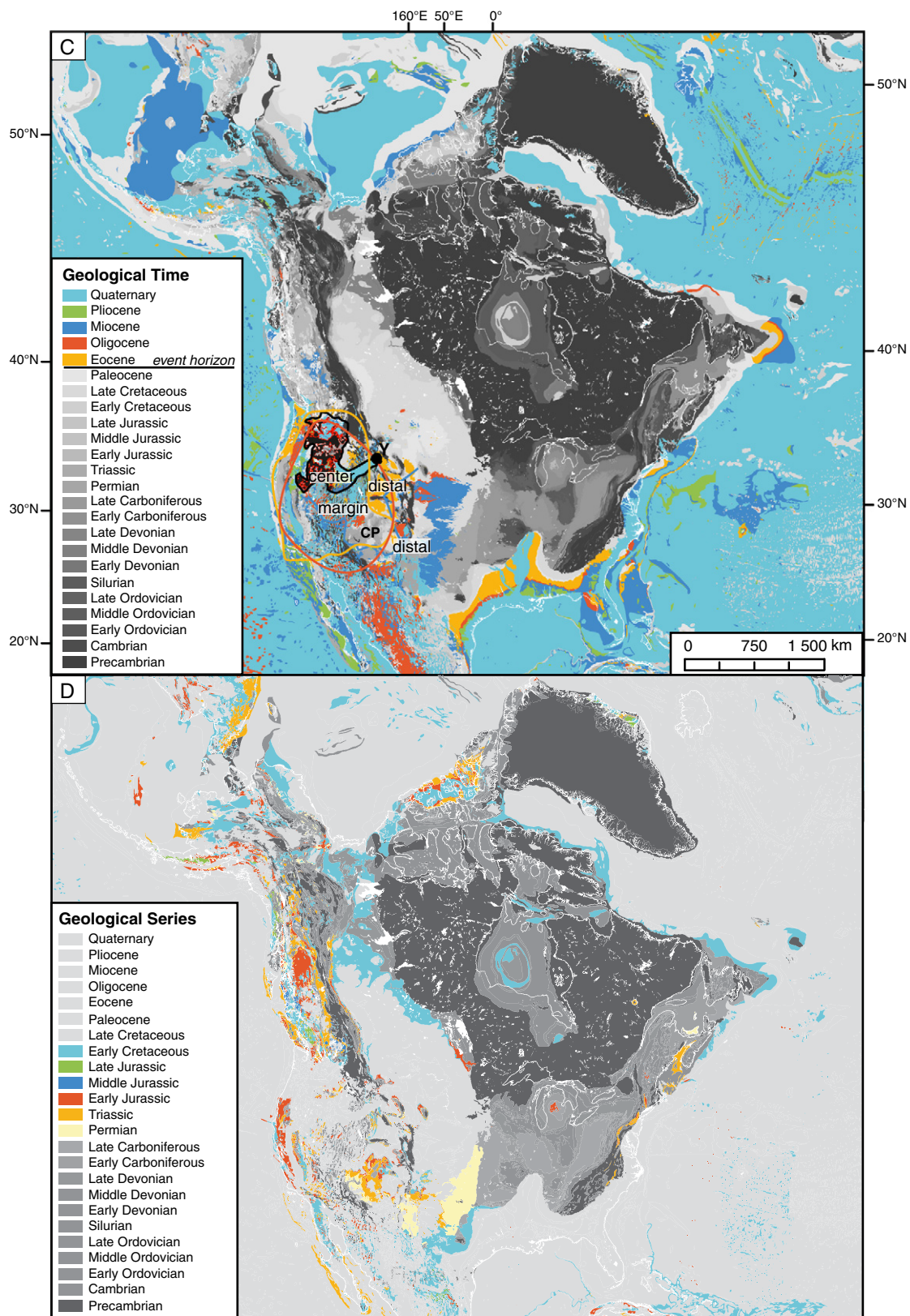


Fig. 12 (continued).

Table 1

Results of plume-stratigraphic mapping of flood basalt provinces discussed in text.

	Flood Basalt Province		
	Deccan	Etendeka-Parana	Columbia River/Yellowstone
Size ^a	600,000 km ² (1,800,000 km ²)	2,000,000 km ²	208,000 km ^{2,c} 210,000 km ^{3,c}
Volume ^a	8 600,000 km ³		
Age (Ma) ^b	66–65	134–132	16.6–15.3
Stage on Fig. 7	F	G	E/F, or F
Age of pre-plume basement rocks exposed below flood basalt	Proterozoic (>541)	Etendeka: >541 Parana: Devonian to Cretaceous	Proterozoic to Cretaceous (deformed strata)
Age of plume-stratigraphic unit 4b below flood basalt	NE-region: Mid-Triassic/Lower Cretaceous	Insufficient map resolution	Miocene
Duration of Hiatus ABC (m.y.)	>480	>409 Ma and c. 67 Ma	50 to >520 Ma
Evidence for elevated dome (uplift and erosion)	Yes. Hiatus ABC; high denudation rates and increased sedimentation rates (Upper Cretaceous) ^e	Etendeka (African side): Yes. Parana: limited. Flood basalts rest on synformal Paleozoic units	Yes. See text. Section 5.3.
Estimated dimension of region affected by plume event	>2000 km, rest is buried under Himalayan foreland basin and Arabian sea ^d	>2000 km; distal extent masked by other plume events in Africa and buried by Andean-related sedimentation in South America.	>1500 km, rest of signal affected oceanic plates now subducted underneath North America
Permissible and viable geological age of event horizon (based on map resolution and patterns)	Base of Cretaceous system	Base of Triassic system	Base of Paleocene series or base of Eocene series
Estimated duration of plume ascent	c. 80 m.y.	c. 120 m.y.	42 or 48 m.y.
Uncertainties and their sources	Tens of millions of years; temporal resolution of units shown on geological maps (systems)	Tens of millions of years; temporal resolution of units shown on geological maps (systems)	Tens of millions of years; temporal resolution of units shown on geological maps (systems)
Temporal resolution of base maps	Insufficient	Insufficient	Partly sufficient

^a Ernst and Buchan (2001a, 2001b).

^b Courtillot and Renne (2003).

^c Reidel et al. (2013).

^d Todal and Edholm (1998).

^e Sahu et al. (2013).

also uplifted and deformed the Farallon plate, both, the oceanic portion and its subducted slab underneath the North American plate (Fig. 13C). Dynamic uplift may have changed the slab geometry depending on the relative position of the rising plume to the descending slab by enhancing either slab roll-back, or slab flattening. If so, numerous crustal geological processes were indirectly affected by it. A definitive answer will also depend on far-field effects related to emplacement of the Iceland plume at c. 57 Ma, which resulted in spreading-rate variations that would also have affected the position of the North American plate relative to its subduction system.

6. Discussion

6.1. The expression of the plume mode on geological maps

Our preliminary plume-stratigraphic mapping of Cenozoic continental examples (Section 5) is generally consistent with features and patterns predicted in Figs. 6 and 7. The diagnostic domes (Şengör, 2001) should be easy to recognize based on their large radius and their major bounding-unconformities (Figs. 6 to 9). Because of the inversion of the plume-marginal region, sediments belonging to this region may be eroded and only preserved as a reworked conformable distal section. The elevated region of Africa and regions in central Asia, and the eastern portion of the Yellowstone plume region may be the best continental candidates to reveal a record of this early phase (Fig. 6A and B). However, this is probably difficult to recognize on most continent-scale geological map unless high temporal-resolution maps on the scale of millions-of-years (geological ages/stages, not epochs/series) are available. Mapping of volcanic rocks, radial dike-swarms, and exposed intrusive rocks will further help to define the plume-stratigraphic framework. Identification of the pre-eruption central sediments (unit 4b) that fill pre-eruption rifts is more difficult, because they are concealed below the flood basalts. Evidence for lateral collapse of the plume head exists for the two youngest continental events, the Iceland plume-head (Barnett-Moore et al., 2017, Data Repository) and the Columbia River event (Fig. 5; Camp et al., 2015). A pulse of asthenospheric flow that

traversed underneath a continent (e.g., Danish-Polish Trough in Europe, Data Repository Fig. DR-2; Basin-and-Range Province, Figs. 12 B, and C) is visible on maps that yield a sufficiently high temporal-resolution of their geological units. The distal conformable successions may be easy to map given the long-lived character of the thermal and isostatic subsidence of tens-to-hundreds-of-million-years following plume-head events under continental lithosphere (Campbell, 2007). Continent-scale and interregional maps should be ideally suited to show these units. Successor basins, such as the one related to the Late Proterozoic Mid-Continent Rift, may have formed this way (Stein et al., 2014).

6.2. Size and duration of plume-head events from geological maps

The effects of uplift, erosion, and sedimentation cover a larger region than typically considered. All three examples presented here reveal systematic patterns around their respective flood basalts and the central dome regions, which are significantly larger than 1000 km, in some cases 2000 km in dimension (Table 1). Şengör (2001) specifically points to this fact in his analysis of the Afar plume. Şengör (2001) recognized that the uplift immediately preceding flood-basalt eruption causes sediment deposition in adjacent regions. In his Fig. 11, he shows a radius for the Afar dome of ca. 1300 km and mapped north-easterly-directed transport for dome-derived Miocene and Pliocene sediment beyond this radius to the Persian Gulf. For the Damman Formation of lower to middle Eocene age, he noted a gradual thickening from the Persian Gulf westwards (see Fig. 12 in Şengör, 2001) as the only evidence for pre-Oligocene activity related to the Afar plume.

Estimates on the duration of the three plume-head events based on preliminary mapping (Figs. 10 to 12) range from 40 to 120 m.y. (Table 1). Uncertainties on these estimates are very large, because the base maps used here yielded a temporal resolution of tens-of-millions-of-years. Geological maps at the resolution of stages would be ideal. Nonetheless, the numbers are consistent with results from numerical modeling (e.g., Colli et al., 2018, in this issue).

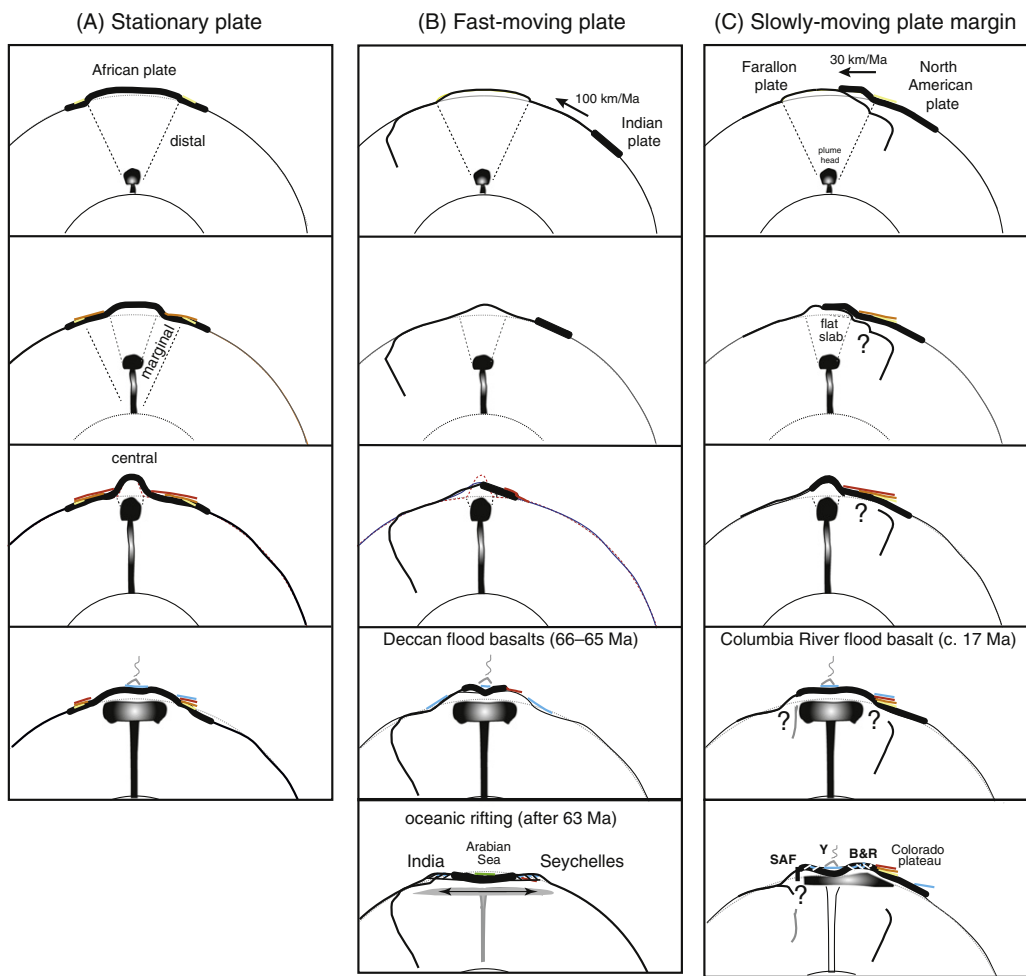


Fig. 13. Sectional drawings showing the temporal and spatial relationships between the plate- and the plume-mode for (a) a stationary plate (Africa), (b) a fast moving plate (India), and (c) a slowly-moving plate above an active subduction zone (North America). SAF – San Andreas fault; Y – Yellowstone; B&R – Basin-and-Range Province.

6.3. Duration of thermal relaxation from geological maps

The 250-Ma-Siberian flood-basalt Province (Data Repository) corresponds to thermal-relaxation status G (Fig. 7), whereas other examples discussed here have not yet reached this status some tens of millions-of-years following the plume events (Table 1). Rainbird and Ernst (2001) state “the initial effects of plume-related uplift are manifested in tens-of-millions-of-years prior to magmatism. In some places, uplift is preserved for hundreds of millions of years afterwards” (Rainbird and Ernst, 2001). Campbell (2001) emphasized that subsidence following melt extraction and eruption of flood basalts may last 500 to 1000 m.y., which could result in the formation of sedimentary basins. One of the best documented recent examples for such long lasting effects is the west Greenland margin related to the North Atlantic igneous-province (Japsen et al., 2006; Fig. 54, time slice 11-Ma in Green et al., 2013). Here, Miocene strata unconformably cover the rifted and uplifted margin. Our plume-stratigraphic maps allow to independently visualize these results (Data Repository). Over 40 m.y. after the eruption of the flood basalts, the Miocene strata are the first (preserved) onlapping successions (Data Repository Fig. DR-2). However, younger pulses of dynamic topography may also result in such unconformities.

6.4. Interaction of plume- and plate-modes

A stationary plate, such as the African plate, records a complete plume-event (Fig. 13A) or a series of plume events (Thiessen et al.,

1979). At least one portion of the distal sedimentary successions may be marine if the central dome is located within about 1500 km of the continental margin.

A fast-moving plate (e.g., India) will not experience, nor record a complete plume-stratigraphic record (Fig. 13B). For example, since c. 120 Ma and until the time of Deccan-basalt eruption, India moved northwards at an accelerating rate of 50 to 150 km/m.y. (Iaffaldano et al., 2011; Nerlich et al., 2016). Therefore, India was not positioned over the rising plume-head until a few m.y. prior to eruption of the Deccan flood basalts (c. 65 Ma; Courtillot et al., 1999; Saunders et al., 2007). Thermochronological studies show that erosional unroofing of Proterozoic basement east of the Deccan traps is restricted to the Late Cretaceous (see Fig. 8 in Sahu et al., 2013). Knowing how much of the surface uplift is due to dynamic topography above the rising plume versus the dynamic topography related to later lateral-spreading of the collapsing plume head will help to place constraints on the relative rate of plume ascent and dispersal (Fig. 13B).

In contrast, if a slowly-moving plate-edge is situated above the incipient plume-head, such as the Cenozoic North American plate-margin (Fig. 13C), the interaction is more complex, and leaves a rich record on the continent as discussed above. The Columbia River/Yellowstone case is highly asymmetric, because half of the early record of the rising plume-head must have affected the Farallon plate west of the convergent margin before the North-American plate moved over dynamically-high topography. This scenario can be reconstructed based on the inferred low-velocity of the North American plate relative to the

plume (Camp, 2013), and on the limited distance over which the continent moved over the trajectory of the plume (Fig. 13C). Half of the plume-margin and the distal stratigraphic records are preserved on the North-American continent east and southeast of the Columbia River dome (Figs. 12 B and C).

Other reasons for asymmetric patterns of uplift and subsidence and sedimentary preservation include inherited lithospheric heterogeneity (West Siberian flood basalt province; Data Repository Fig. DR-1; European plume margin DR-2) and the proximity to former long-lived subduction systems (e.g., central and southern South America). These factors exert control whether or not a dome forms and whether or not the surrounding regions are uniformly affected by lateral spreading of the plume head.

6.5. Ratio of conformable to unconformable contacts and implications for geodynamics

The ratio between conformable and unconformable contacts on a global scale appears to have been quite constant – between 20 and 30% – throughout the Phanerozoic, suggesting that at any given system-boundary, 20–30% of the earth's surface is affected by significant interregional hiatus-forming processes, i.e., hiatuses tens-of-m.y. in duration and on interregional scales (Fig. 3). Eustatic fluctuations result in hiatuses, but not at the scale of geological systems. For example, the distribution of conformable and unconformable contacts for the K/T-system-boundary broadly correlates with regions of long-lived subduction systems and regions of mantle upwelling, respectively (Fig. 3B); Most of the Mediterranean/Tethyan region and a large fraction of the Pacific ring expose conformable K/T-boundaries. In contrast, Central and North America, yield non-conformable K/T-boundaries. Specifically, Cretaceous basin inversions, represented by Tertiary units that rest unconformably on Jurassic units (Fig. DR-5B) are concentrated in the vicinity of rising plumes (Columbia, Iceland, and Afar). Over Phanerozoic time, North America shows fluctuations in this ratio, which mimic the Sloss-sequence pattern (Fig. 3A and Fig. DR-5A; e.g., Sloss et al., 1949). In agreement with Burgess and Gurnis (1995), we infer that long-lived zones of subduction keep continents low for long periods of time and over large regions. The upward-directed motion of the mantle, i.e., the plume-mode, directly results in interregional-scale unconformities as the only significant process that can produce and preserve such significant hiatuses in continental interiors and near plate-boundaries.

This would imply a significant contribution of mantle plumes to earth dynamics. Classical estimates derived from flood basalts and local bathymetric swells put the heat coming from the core-mantle boundary in the range of 5 to 15% of the mantle heat budget (see e.g., Davies, 1988a; Sleep, 1990). A stronger contribution in the range of 30%, inferred from theoretical considerations of compressibility effects and the non-adiabatic mantle geotherm (e.g., Bunge, 2005; Schuberth et al., 2009a, 2009b; Simmons et al., 2009), would instead agree well with the geologic signal (Fig. 3 and Fig. DR-5). This ratio is also reflected by the Phanerozoic distribution of continental (30%) versus oceanic (70%) surface area on the earth.

The size of the dynamic topography signal induced by the plume mode is of interregional scale, in contrast to the very long-wavelength dynamic-topography signal of the plate mode. A superposition of plate- and plume-mode dynamic topography would yield a complex interference signal, which may help to explain why recent global dynamic-topography-estimates based on backstripping of stratigraphic successions obtained from seismic surveys (Hoggard et al., 2017) are at odds with dynamic-topography predictions derived from global geodynamic models where the plate mode is commonly assumed to be dominant.

An extensive and accurate mapping of plume-related topography and its change over time could help illuminate the extent to which the plume mode contributes to plate-tectonic driving forces and intraplate

seismic hazards, for example through rapid plate-motion variations (Iaffaldano and Bunge, 2015), i.e., plate motion changes that occur on short time-scales relative to a mantle overturn. Such changes are increasingly revealed by high temporal-resolution plate reconstructions (Iaffaldano et al., 2014). Colli et al. (2014) link South Atlantic spreading-rate changes explicitly with regional dynamic-topography changes through variations in pressure-driven upper-mantle flow. Moreover, mass displacements induced by the plume mode may also occur sufficiently fast to be detectable by current and future gravity missions (e.g., Ghelichkhan et al., 2018-in this issue). Linking plume-mode signals from geodetic to geologic time scales (e.g., Friedrich et al., 2003) may thus become feasible through geodynamic models employing inverse techniques (e.g. Colli et al., 2018, in this issue). These links across scales would provide powerful constraints on dynamic earth models, supporting their use in studies that link solid earth and climate processes (e.g., Austermann and Mitrovica, 2015; Baran et al., 2014).

7. Conclusions

We proposed an event-based plume-stratigraphic framework to identify the full surface expression of the plume mode, and to untangle the effects of overlapping plume- and plate-mode. Based on the first-order assessment of interregional-scale geological maps that were not compiled for this purpose, basic patterns emerge that are consistent with mantle-geodynamic principles. The plume mode affects the geological record far beyond domes and flood basalts; The plume margins record transient and complex interaction of lithospheric and surface processes, and a distal sedimentary record hypothetically documents the whole event. The interpretation of such features should occur in the context of event-based stratigraphic frameworks in addition to those used to map plate tectonic features and corrected for eustatic sea-level fluctuations. Our proposed plume-stratigraphic framework for plate interiors should be tied to orogenic (plate boundary) stratigraphy to complete the global stratigraphic synthesis; Empirical stratigraphy is not useful for this purpose.

Inherited lithospheric-heterogeneities control kinematic boundary conditions locally and affect the evolution of a plume's surface expression. Interference of plume- and plate-mode processes is expected beyond a simple linear superposition of the two modes and results in unique geological features, such as those encountered in the western United States. While the vertical and horizontal speed of both plate- and plume-mode may be similar, the duration and spatial dimensions of their surface expression are different. Compilations of interregional geological maps therefore need to provide a temporal resolution of epochs/series and ages/stages that allow visualization of process rates at km/m.y.

The largest unknown is the speed and duration of plume-head rising. In a planet with an isoviscous mantle, such as the one modeled by Griffiths et al. (1989) on which we based our plume-stratigraphic framework, dynamic topography of the planetary surface sets in with plume initiation. However, given the earth's non-isoviscous mantle structure, the appearance of dynamic topography may be subdued until the plume enters into the highest low-viscosity layer within the mantle. The plume-stratigraphic framework developed here applies equally to an asthenosphere-bearing mantle. However, the surface expression of the “below-asthenospheric phase” of the rising plume would impact only the longest wavelengths, thus requiring geological data visualization of stages/ages on interregional to continental-scale maps.

Unconformity analysis of geological maps revealed that transient unconformable system-boundaries occur at a constant 20 to 30% throughout the Phanerozoic. Our plume-stratigraphic analysis of interregional geological maps showed that the largest of these unconformable contacts form in association with dynamic topography above mantle plumes, which results in significant uplift and erosion on interregional scales. No other process on the earth may be able to generate

erosion on such scales. However, uplift is limited to interregional scales and none of these processes are capable of producing any global-scale unconformities.

Visualization of hialt surfaces as proxies for dynamic topography and their comparison to numerical results requires map compilation and digital analysis at a technical level. For this purpose, we suggest to reconstruct sequential, uncovered paleogeographic maps of geological and stratigraphic records with event-based and/or diverging colors-schemes at high temporal resolution.

Supplementary data to this article can be found online at <http://dx.doi.org/10.1016/j.gr.2017.06.003>.

Acknowledgments

This research did not receive any specific grant from funding agencies in the public, commercial, or not-for-profit sectors. We thank Sara Carena, A.M. Celal Sengör, and an anonymous reviewer for constructive comments.

References

- Al-Hajri, Y., White, N., Fishwick, S., 2009. Scales of transient convective support beneath Africa. *Geology* 37 (10), 883–886.
- Amante, C., Eakins, B.W., 2009. ETOPO1 1 Arc-Minute Global Relief Model: procedures, data sources and analysis. NOAA Technical Memorandum NESDIS NGDC-24. National Geophysical Data Center, NOAA <http://dx.doi.org/10.7289/V5C8276M>.
- Asch, K., 2003. The 1:5 Million International Geological Map of Europe and Adjacent Areas: Development and Implementation of a GIS-enabled Concept. *Geologisches Jahrbuch, SA* 3, Stuttgart: E. Schweizerbart, Sonderheft A3. SA 3 p. 172.
- Atwater, T., 1970. Implications of plate tectonics for the Cenozoic tectonic evolution of western North America. *Geological Society of America Bulletin* 81 (12):3513–3536. [http://dx.doi.org/10.1130/0013-4470\(1970\)81\[3513:OPTFT\]2.0.CO;2](http://dx.doi.org/10.1130/0013-4470(1970)81[3513:OPTFT]2.0.CO;2).
- Austermann, J., Mitrovica, J.X., 2015. Calculating gravitationally self-consistent sea level changes driven by dynamic topography. *Geophysical Journal International* 203: 1909–1922. <http://dx.doi.org/10.1093/gji/ggv371>.
- Baksi, A.K., 1994. Geochronological studies on whole-rock balsats, Deccan Traps, India: evaluation of the timing of volcanism relative to the K-T boundary. *EPSL* 121, 43–56.
- Baran, R., Friedrich, A.M., Schlunegger, F., 2014. The late Miocene to Holocene erosion pattern of the Alpine foreland basin reflects Eurasian slab unloading beneath the western Alps rather than global climate change. *Lithosphere* 6 (2), 124–131.
- Barnett-Moore, N., Hassan, R., Flament, N., Müller, R.D., 2017. The deep Earth origin of the Iceland plume and its effects on regional uplift and subsidence. *Solid Earth* 8: 235–254. <http://dx.doi.org/10.5194/se-8-235-2017>.
- Belousov, V.V., 1962. Basic problems in geotectonics. In: Shrock, R.R. (Ed.), *International Series in the Earth Sciences*. McGraw-Hill Book Company, Inc., New York.
- Bennett, R.A., Wernicke, B.P., Niemi, N.A., Friedrich, A.M., Davis, J.L., 2003. Contemporary strain rates in the northern Basin and Range province from GPS data. *Tectonics* 22: 1008. <http://dx.doi.org/10.1029/2001TC001355>.
- Bernet, M., Spiegel, C. (Eds.), 2004. *Detrital Thermochronology*. Geological Society of America Special Paper 378 (126 pp.).
- Best, M.G., Gromme, S., Deino, A.L., Christiansen, E.H., Hart, G.L., Tingey, D.G., 2013. The 36–18 Ma Central Nevada ignimbrite field and calderas, Great Basin, USA: multicyclic super-eruptions. *Geosphere* 9 (6):1562–1636. <http://dx.doi.org/10.1130/GES00945.1>.
- Boyden, J.A., Müller, R.D., Gurnis, M., Torsvik, T.H., Clark, J.A., Turner, M., Ivey-Law, H., Watson, R.J., Cannon, J.S., 2011. Next-generation plate-tectonic reconstructions using GPlates. *Geoinformatics: Cyberinfrastructure for the Solid Earth Sciences*. 9. Cambridge University Press, Cambridge, UK, pp. 5–114.
- Bunge, H.-P., 2005. Low plume excess temperature and high core heat flux inferred from non-adiabatic geotherms in internally heated mantle circulation models. *Physics of the Earth and Planetary Interiors* 153 (1–3):3–10. <http://dx.doi.org/10.1016/j.pepi.2005.03.017>.
- Bunge, H.-P., Richards, M.A., Baumgardner, J.R., 1996. Effect of depth-dependent viscosity on the planform of mantle convection. *Nature* 379 (6564):436–438. <http://dx.doi.org/10.1038/379436a0>.
- Bunge, H.-P., Richards, M.A., Lithgow-Bertelloni, C., Baumgardner, J.R., Grand, S.P., Romanowicz, B.A., 1998. Time scales and heterogeneous structure in geodynamic earth models. *Science* 280:91–95. <http://dx.doi.org/10.1126/science.280.5360.91>.
- Bunge, H.-P., Hagelberg, C.R., Travis, B.J., 2003. Mantle circulation models with variational data assimilation: inferring past mantle flow and structure from plate motion histories and seismic tomography. *Geophysical Journal International* 152:280–301. <http://dx.doi.org/10.1046/j.1365-246X.2003.01823.x>.
- Burgess, P.M., Gurnis, M., 1995. Mechanisms for the formation of cratonic stratigraphic sequences. *EPSL* 136 (3–4):647–663. [http://dx.doi.org/10.1016/0013-821X\(95\)00204-P](http://dx.doi.org/10.1016/0013-821X(95)00204-P).
- Burgess, P.M., Gurnis, M., 1995. Mechanisms for the formation of cratonic stratigraphic sequences. *Earth and Planetary Science Letters* 136 (3–4), 647–663.
- Burke, K., Dewey, J.F., 1973. Plume-generated triple junctions: key indicators in applying plate tectonics to old rocks. *Journal of Geology* 81:406–433. <http://dx.doi.org/10.1086/627882>.
- Burke, K., Gunnell, Y., 2008. The African erosion surface: a continental-scale synthesis of geomorphology, tectonics, and environmental change over the past 180 million years. *Geological Society of America Memoirs* 201, 1–66.
- Burke, K., Wilson, J.T., 1972. Is the African plate stationary? *Nature* 239:387–390. <http://dx.doi.org/10.1038/239387b0>.
- Busby, C.J., Ingersoll, R.V. (Eds.), 1995. *Tectonics of Sedimentary Basins*. Blackwell Science, Cambridge, MA (ISBN 0-86542-245-1).
- Camp, V.E., 1995. Mid-Miocene propagation of the Yellowstone mantle plume head beneath the Columbia River basalt source region. *Geology* 23 (5):435–438. [http://dx.doi.org/10.1130/0091-7613\(1995\)023<0435:MMPT>2.3.CO;2](http://dx.doi.org/10.1130/0091-7613(1995)023<0435:MMPT>2.3.CO;2).
- Camp, V.E., 2013. Origin of Columbia River basalt: passive rise of shallow mantle, or active upwelling of a deep-mantle plume? *Geological Society of America Special Papers* 497:181–199. <http://dx.doi.org/10.1130/9780813724973>.
- Camp, V.E., Ross, M.E., 2004. Mantle dynamics and genesis of mafic magmatism in the intermontane Pacific Northwest. *Journal of Geophysical Research: Solid Earth* 109 (B8). <http://dx.doi.org/10.1029/2003JB002838>.
- Camp, V.E., Pierce, K.L., Morgan, L.A., 2015. Yellowstone plume trigger for Basin and Range extension, and coeval emplacement of the Nevada–Columbia Basin magmatic belt. *Geosphere* 11 (2):203–225. <http://dx.doi.org/10.1130/GES01051.1>.
- Campbell, I.H., 2001. Identification of ancient mantle plumes. *Geological Society of America Special Papers* 352:5–21. <http://dx.doi.org/10.1130/0-8137-2352-3.5>.
- Campbell, I.H., 2007. Testing the plume theory. *Chemical Geology* 241:153–176. <http://dx.doi.org/10.1016/j.chemgeo.2007.01.024>.
- Campbell, I.H., Griffiths, R.W., 1990. Implications of mantle plume structure for the evolution of flood basalts. *Earth and Planetary Science Letters* 99:79–93. [http://dx.doi.org/10.1016/0012-821X\(90\)90072-6](http://dx.doi.org/10.1016/0012-821X(90)90072-6).
- Catuneanu, O., 2006. *Principles of Sequence Stratigraphy*. Elsevier, p. 386.
- Chase, C.G., Sproul, D.R., 1983. The modern geoid and ancient plate boundaries. *Earth and Planetary Science Letters* 62:314–320. [http://dx.doi.org/10.1016/0012-821X\(83\)90002-X](http://dx.doi.org/10.1016/0012-821X(83)90002-X).
- Christie-Blick, N., Mountain, G.S., Miller, K.G., 1990. Seismic stratigraphic record of sea level change. *Sea-level Change*. National Academy of Sciences Studies in Geophysics. National Academy Press, Washington, D.C., pp. 116–140.
- Coe, A.L., 2002. *The Sedimentary Record of Sea-level Change*. Cambridge University Press (287 pp.).
- Colgan, J.P., Dumitru, T.A., Miller, E.L., 2004. Diachroneity of Basin and Range extension and Yellowstone hotspot volcanism in northwestern Nevada. *Geology* 32, 121–124.
- Colli, L., Stotz, I., Bunge, H.-P., Smethurst, M.A., Clark, S., Iaffaldano, G., Tassara, A., Guilloucheau, F., Bianchi, M.C., 2014. Rapid South Atlantic spreading changes and coeval vertical motion in surrounding continents: evidence for temporal changes of pressure-driven upper mantle flow. *Tectonics* 33:1304–1321. <http://dx.doi.org/10.1029/2014TC003612>.
- Colli, L., Ghelichkhan, S., Bunge, H.-P., 2016. On the ratio of dynamic topography and gravity anomalies in a dynamic Earth. *Geophysical Research Letters* 43:2510–2516. <http://dx.doi.org/10.1002/2016GL067929>.
- Colli, L., Ghelichkhan, S., Bunge, H.-P., Oeser, J., 2018. Retroductions of Mid Paleogene mantle flow and dynamic topography in the Atlantic region from compressible high resolution adjoint mantle convection models: Sensitivity to deep mantle viscosity and tomographic input model. *Gondwana Research* 53, 252–272 (in this issue).
- Commission for the Geological Map of the World, Bouysse, P., 2014. *Geological Map of the World: 35 000 000, CGMW/UNESCO*.
- Coney, P.J., 1978. Mesozoic-Cenozoic Cordilleran plate tectonics. *Geological Society of America Memoirs* 152, 33–50.
- Conrad, C.P., 2013. The solid Earth's influence on sea level. *Geological Society of America Bulletin* 125 (7–8), 1027–1052.
- Courtillot, V.E., Renne, P.R., 2003. On the ages of flood basalt events. *Comptes Rendus Geosciences* 313:113–140. [http://dx.doi.org/10.1016/S1631-0713\(03\)00006-3](http://dx.doi.org/10.1016/S1631-0713(03)00006-3).
- Courtillot, V., Jaupart, C., Manighetti, I., Tapponnier, P., Besse, J., 1999. On causal links between flood basalts and continental breakup. *Earth and Planetary Science Letters* 166 (3):177–195. [http://dx.doi.org/10.1016/S0012-821X\(98\)00282-9](http://dx.doi.org/10.1016/S0012-821X(98)00282-9).
- Cox, K.G., 1989. The role of mantle plumes in the development of continental drainage patterns. *Nature* 342:873–877. <http://dx.doi.org/10.1038/342873a0>.
- Crough, S.T., 1979. Hotspot epirogeny. *Tectonophysics* 61 (1–3):321–333. [http://dx.doi.org/10.1016/0040-1951\(79\)90304-4](http://dx.doi.org/10.1016/0040-1951(79)90304-4).
- Dasgupta, A.K., Ghose, A., Chakraborty, K.S., 1993. *Geological Map of India: Hyderabad, Geological Survey of India, Scale 1: 5 000 000*.
- Davies, G.F., 1988a. Ocean bathymetry and mantle convection 1. Large-scale flow and hotspots. *Journal of Geophysical Research* 93 (B9):10467–10480. <http://dx.doi.org/10.1029/JB093iB09p10467>.
- Davies, G.F., 1988b. Ocean bathymetry and mantle convection 2. Small-scale flow. *Journal of Geophysical Research* 93 (B9):10481–10488. <http://dx.doi.org/10.1029/JB093iB09p10481>.
- Davies, G.F., 1999. *Dynamic Earth: Plates, Plumes and Mantle Convection*. Cambridge University Press <http://dx.doi.org/10.1017/CBO9780511605802>.
- Davies, J.H., Bunge, H.-P., 2006. Are splash plumes the origin of minor hotspots? *Geology* 34 (5):349–352. <http://dx.doi.org/10.1130/G22193.1>.
- Davies, J.H., Davies, D.R., 2010. *Earth's surface heat flux*. *Solid Earth* 1, 5–24.
- Davies, G.F., Richards, M.A., 1992. Mantle convection. *The Journal of Geology* 100: 151–206. <http://dx.doi.org/10.1086/629582>.
- Davies, D.R., Goes, S., Lau, H.C.P., 2015. Thermally Dominated Deep Mantle LLSPs: A Review. Springer International Publishing, Cham:pp. 441–477 http://dx.doi.org/10.1007/978-3-319-15627-9_14.

- Dewey, J.F., 1982. Plate tectonics and the evolution of the British Isles. *Journal of the Geological Society* 139:371–412. <http://dx.doi.org/10.1144/gsjgs.139.4.0371>.
- Dunbar, C.O., Rodgers, J., 1957. *Principles of Stratigraphy*. Wiley, New York (356 pp).
- Duncan, R.A., Richards, M.A., 1991. Hotspots, mantle plumes, flood basalts, and true polar wander. *Reviews of Geophysics* 29:31–50. <http://dx.doi.org/10.1029/90RG02372>.
- Dutton, C.E., 1876. Critical observations on theories of the Earth's physical evolution. *Geological Magazine Series 2* (3), 322–328.
- Dutton, C.E., 1880. Report on the Geology of the High Plateaus of Utah, With Atlas, Department of the Interior, U.S. Geographical and Geological Survey of the Rocky Mountain Region, J.W. Powell in Charge. Government Printing Office, Washington (307 pp).
- Ebinger, C.J., Sleep, N.H., 1998. Cenozoic magmatism throughout east Africa resulting from impact of a single plume. *Nature* 395:788–791. <http://dx.doi.org/10.1038/27417>.
- Engebretson, D.C., Cox, A., Gordon, R.G., 1985. Relative Motions Between Oceanic and Continental Plates in the Pacific Basin. *Geological Society of America Special Paper* 206 (59 pp).
- Ernst, R.E., Buchan, K.L., 2001a. Mantle Plumes: Their Identification Through Time. *Geological Society of America Special Paper* 593 pp.
- Ernst, R.E., Buchan, K.L., 2001b. Large mafic magmatic events through time and links to mantle-plume heads. In: Ernst, R.E., Buchan, K.L. (Eds.), *Mantle Plumes: Their Identification Through Time*. Geological Society of America Special Paper 352, pp. 483–576.
- Ernst, R.E., Buchan, K.L., 2001c. The use of mafic dike swarms in identifying and locating mantle plumes. In: Ernst, R.E., Buchan, K.L. (Eds.), *Mantle plumes: Their identification through time*. Geological Society of America Special Paper 352, pp. 247–265.
- Ernst, R.E., Buchan, K.L., 2002. Maximum size and distribution in time and space of mantle plumes: evidence from large igneous provinces. *Journal of Geodynamics* 34 (2): 309–342. [http://dx.doi.org/10.1016/S0264-3707\(02\)00025-X](http://dx.doi.org/10.1016/S0264-3707(02)00025-X).
- von Eynatten, H., Dunkl, I., 2012. Assessing the sediment factory: the role of single grain analysis. *Earth-Science Reviews* 115 (1), 97–120.
- Farnetani, C.G., Richards, M.A., 1994. Numerical investigations of the mantle plume initiation model for flood basalt events. *Journal of Geophysical Research* 99: 13813–13833. <http://dx.doi.org/10.1029/94JB00649>.
- Fisher, O., 1889. *Physics of the Earth's Crust*. 2nd ed. Macmillan and Company, London, p. 391.
- Flowers, R.M., Wernicke, B.P., Farley, K.A., 2008. Unroofing, incision, and uplift history of the southwestern Colorado Plateau from apatite (U-Th)/He thermochronometry. *Geological Society of America Bulletin* 120 (5–6):571–587. <http://dx.doi.org/10.1130/B26231.1>.
- French, S.W., Romanowicz, B.A., 2014. Whole-mantle radially anisotropic shear velocity structure from spectral-element waveform tomography. *Geophysical Journal International* 199:1303–1327. <http://dx.doi.org/10.1093/gji/ggu334>.
- Friedrich, A.M., Wernicke, B.P., Niemi, N.A., Bennett, R.A., Davis, J.L., 2003. Comparison of geodetic and geologic data from the Wasatch region, Utah, and implications for the spectral character of Earth deformation at periods of 10 to 10 million years. *Journal of Geophysical Research: Solid Earth* 108 (B4). <http://dx.doi.org/10.1029/2001JB000682>.
- Friedrich, A.M., Lee, J., Wernicke, B.P., Sieh, K., 2004. Geologic context of geodetic data across a Basin and Range normal fault, Crescent Valley, Nevada. *Tectonics* 23, TC2015. <http://dx.doi.org/10.1029/2003TC001528>.
- Galloway, W.E., Whiteaker, T.L., Ganey-Curry, P., 2011. History of Cenozoic north American drainage basin evolution, sediment yield, and accumulation in the Gulf of Mexico basin. *Geological Society of America Bulletin* 7, 938–973.
- Ghelichkhan, S., Bunge, H.-P., 2016. The compressible adjoint equations in geodynamics: derivation and numerical assessment. *GEM: International Journal on Geomathematics* 7 (1):1–30. <http://dx.doi.org/10.1007/s13137-016-0080-5>.
- Ghelichkhan, S., Murböck, M., Colli, L., Pail, R., Bunge, H.-P., 2018. On the observability of epeirogenic movement in current and future gravity missions. *Gondwana Research* 53, 273–284 (in this issue).
- Gordon, R.G., Jurdy, D.M., 1986. Cenozoic global plate motions. *Journal of Geophysical Research* 91:12389–12406. <http://dx.doi.org/10.1029/JB091iB12p12389>.
- Gradstein, F., Ogg, J., 2004. Geologic Time Scale 2004 – why, how, and where next! *Lethaia* 37 (2):175–181. <http://dx.doi.org/10.1080/00241160410006483>.
- Gradstein, F., Ogg, J., Smith, A., 2004. *A Geologic Time Scale 2004*. Cambridge Press, p. 589.
- Gradstein, F., Ogg, J., Schmitz, M.D., Ogg, G.M., 2012. *The Geologic Time Scale 2012*. Elsevier (1176 pp. (2 vol.)).
- Green, P.F., Lidmar-Bergström, K., Japsen, P., Bonow, J.M., Chalmers, J.A., 2013. Stratigraphic landscape analysis, thermochronology and the episodic development of elevated, passive continental margins. *Geological Survey of Denmark and Greenland Bulletin* 30 (150), 2013.
- Green, P.F., Japsen, P., Chalmers, J.A., Bonow, J.M., Duddy, I.R., 2017. Post-breakup burial and exhumation of passive continental margins: nine propositions to inform geodynamic models. *Gondwana Research* 53, 58–81 (in this issue).
- Griffiths, R.W., Campbell, I.H., 1990. Stirring and structure in mantle starting plumes. *Earth and Planetary Science Letters* 99:66–78. [http://dx.doi.org/10.1016/0012-821X\(90\)90071-5](http://dx.doi.org/10.1016/0012-821X(90)90071-5).
- Griffiths, R.W., Gurnis, M., Eitelberg, G., 1989. Holographic measurements of surface topography in laboratory models of mantle hotspots. *Geophysical Journal International* 96:477–495. <http://dx.doi.org/10.1111/j.1365-246X.1989.tb06009.x>.
- Guillocheau, F., Simon, B., Baby, G., Bessin, P., Robin, C., Dauteuil, O., 2018. Planation surfaces as a record of mantle dynamics: The case example of Africa. *Gondwana Research* 53, 82–98 (in this issue).
- Hager, B.H., Gurnis, M., 1987. Mantle convection and the state of the Earth's interior. *Reviews of Geophysics* 25:1277–1285. <http://dx.doi.org/10.1029/RG025i006p01277>.
- Hartley, R.A., Roberts, G.G., White, N.J., Richardson, C., 2011. Transient convective uplift of an ancient buried landscape. *Nature Geoscience* 4:562–565. <http://dx.doi.org/10.1038/ngeo1191>.
- Heine, C., Zoethout, J., Müller, R.D., 2013. Kinematics of the South Atlantic Rift. *Solid Earth Discussions* 4:215–253. <http://dx.doi.org/10.5194/se-4-215-2013>.
- Henry, C.D., Hinz, N.H., Faulds, J.E., Colgan, J.P., John, D.A., Brooks, E.R., Cassel, E.J., Garside, L.J., Davis, D.A., Castor, S.B., 2012. Eocene-Early Miocene paleotopography of the Sierra Nevada-Great Basin-Nevadaplano based on widespread ash-flow tuffs and paleovalleys. *Geosphere* 8 (1):1–27. <http://dx.doi.org/10.1130/GES00727.1>.
- Hinderer, M., 2012. From gullies to mountain belts: a review of sediment budgets at various scales. *Sedimentary Geology* 280, 21–59.
- Hoggard, M.J., Winterbourne, J., Czarnota, K., White, N., 2017. Oceanic Residual Depth Measurements, the Plate Cooling Model, and Global Dynamic Topography. *Journal of Geophysical Research: Solid Earth* Wiley-Blackwell <http://dx.doi.org/10.1002/2016jb013457>.
- Hooper, P.R., Camp, V.E., Reidel, S.P., Ross, M.E., 2007. The Columbia River Basalts and their relationship to the Yellowstone hotspot and Basin and Range extension. *Plumes, Plates, and Planetary Processes*. Geological Society of America Special Paper 430, pp. 635–668.
- Iaffaldano, G., Bunge, H.-P., 2015. Rapid plate motion variations through geological time: observations serving geodynamic interpretation. *Annual Review of Earth and Planetary Sciences* 43:571–592. <http://dx.doi.org/10.1146/annurev-earth-060614-105117>.
- Iaffaldano, G., Husson, L., Bunge, H.-P., 2011. Monsoon speeds up Indian plate motion. *EPSL* 304:503–510. <http://dx.doi.org/10.1016/j.epsl.2011.02.026>.
- Iaffaldano, G., Hawkins, R., Bodin, T., Sambridge, M., 2014. REDBACK: open-source software for efficient noise-reduction in plate kinematic reconstructions. *Geochemistry, Geophysics, Geosystems* 15:1663–1670. <http://dx.doi.org/10.1002/2014gc005309>.
- Irving, R.D., 1888. Classification of Early Cambrian and Precambrian Formations. In: Powell, J.W. (Ed.), *Seventh Annual Report of the United States Geological Survey to the Secretary of the Interior 1885–86*. Washington Government Printing Office, pp. 371–454.
- Japsen, P., 2018. Sonic velocity of chalk, sandstone and marine shale controlled by effective stress: Velocity-depth anomalies as a proxy for vertical movements. *Gondwana Research* 53, 145–158 (in this issue).
- Japsen, P., Bonow, J.M., Green, P.F., Chalmers, J.A., Lidmar-Begström, K., 2006. Elevated passive continental margins: long-term highs or Neogene uplifts? New evidence from West Greenland. *Earth and Planetary Science Letters* 248 (1), 300–339.
- Japsen, P., Bonow, J.M., Green, P.F., Cobbold, P.R., Chiossi, D., Lilletveit, R., Magnavita, L.P., Pedreira, A., 2012a. Episodic burial and exhumation in NE Brazil after opening of the South Atlantic. *The Geological Society of America Bulletin* 124:800–816. <http://dx.doi.org/10.1130/B30515.1>.
- Japsen, P., Chalmers, J.A., Green, P.F., Bonow, J.M., 2012b. Elevated, passive continental margins: not rift shoulders, but expressions of episodic, post-rift burial and exhumation. *Global and Planetary Change* 90–91:73–86. <http://dx.doi.org/10.1016/j.gloplacha.2011.05.004>.
- Karlstrom, K.E., Coblenz, D., Dueker, K., Ouimet, W., Kirby, E., Van Wijk, J., Schmandt, B., Kelley, S., Lazear, G., Crossey, L.J., Crow, R., Aslan, A., Darling, A., Aster, R., MacCarthy, J., Hansen, S.M., Stachnik, J., Stockli, D.F., Garcia, R.V., Hoffman, M., McKeon, R., Feldman, J., Heizler, M., Donahue, M.S., 2012. Mantle-driven dynamic uplift of the Rocky Mountains and Colorado Plateau and its surface response: toward a unified hypothesis. *Lithosphere* 4 (1):3–22. <http://dx.doi.org/10.1130/L150.1>.
- Kincaid, C., Druken, K.A., Griffiths, R.W., Stegman, D.R., 2013. Bifurcation of the Yellowstone plume driven by subduction-induced mantle flow. *Nature Geoscience* 6: 395–399. <http://dx.doi.org/10.1038/ngeo1774>.
- Krenkel, E., 1922. Die Bruchzonen Ostafrikas. *Geologische Rundschau* 14 (3), 209–232.
- Krenkel, E., 1925. Die Geologie Afrikas. Erster Teil, Gebrüder Bornträger (461 pp).
- Krenkel, E., 1926. Magmatische Hebungen in Ostafrika. *Centralblatt für Mineralogie, Geologie und Paläontologie B* (2), 50–57.
- Kukla, P.A., Strozyk, F., Mohriak, W.U., 2018. South Atlantic salt basins – Witnesses of complex passive margin evolution. *Gondwana Research* 53, 41–57 (in this issue).
- Lemcke, K., 1974. Vertikalgewegungen des vormesozoischen Sockels im nördlichen Alpenvorland Pern bis zur Gegenwart? *Elogiae Geologicae Helveticae* 67, 121–133.
- Lipman, P.W., Prostka, H.J., Christiansen, R.L., 1971. Evolving subduction zones in the western United States, as interpreted from igneous rocks. *Science* 174 (4011): 821–825. <http://dx.doi.org/10.1126/science.174.4011.821>.
- Lithgow-Bertelloni, C., Richards, M.A., 1998. The dynamics of Cenozoic and Mesozoic plate motions. *Reviews of Geophysics* 36:27–78. <http://dx.doi.org/10.1029/97RG02282>.
- Lovell, B., 2010. A pulse in the planet: regional control of high-frequency changes in relative sea level by mantle convection. *Journal of the Geological Society of London* 167:637–648. <http://dx.doi.org/10.1144/67492009-127>.
- Lyell, C., 1833. *Principles of Geology*. 3rd volume. Murray, London.
- Macgregor, D.S., 2012. Late Cretaceous-Cenozoic sediment and turbidite reservoir supply to South Atlantic margins. *Geological Society, London, Special Publications* 369 (1): 109–128. <http://dx.doi.org/10.1144/SP369.7>.
- Mahoney, J., 1988. Deccan traps. In: MacDougall, J.D. (Ed.), *Continental Flood Basalts*. Kluwer Academic Publishers, pp. 155–194.
- Matthews, K.J., Maloney, K.T., Zahirovic, S., Williams, S.E., Seton, M., Müller, D., 2016. Global plate boundary evolution and kinematics since the late Paleozoic. *Global and Planetary Change* 146:226–250. <http://dx.doi.org/10.1016/j.gloplacha.2016.10.002>.
- McKenzie, D.P., 1977. Surface deformation, gravity anomalies and convection. *Geophysical Journal International* 48:211–238. <http://dx.doi.org/10.1111/j.1365-246X.1977.tb0297x>.
- McQuarrie, N., Wernicke, B.P., 2005. An animated tectonic reconstruction of southwestern North America since 36 Ma. *Geosphere* 1 (3):147–172. <http://dx.doi.org/10.1130/GES00016.1>.
- Miall, A., 2010. *The Geology of Stratigraphic Sequences*. 2nd edition. Springer (522 pp).
- Miller, K.G., Komink, M.A., Browning, J.V., Wright, J.D., Mountain, G.S., Katz, M.E., ... Pekar, S.F., 2005. The Phanerozoic record of global sea-level change. *Science* 310 (5752), 1293–1298.

- Morgan, W.J., 1965. Gravity anomalies and convection currents: 1. A sphere and cylinder sinking beneath the surface of a viscous fluid. *Journal of Geophysical Research* 70: 6175–6187. <http://dx.doi.org/10.1029/JZ070i024p06175>.
- Moucha, R., Forte, A.M., 2011. Changes in African topography driven by mantle convection. *Nature Geoscience* 4:707–712. <http://dx.doi.org/10.1038/ngeo1235>.
- Moucha, R., Forte, A.M., Mitrovica, J.X., Rowley, D.B., Quere, S., Simmons, N.A., Grand, S.P., 2008. Dynamic topography and long-term sea-level variations: there is no such thing as a stable continental platform. *EPSL* 271:101–108. <http://dx.doi.org/10.1016/j.epsl.2008.03.056>.
- Muckherjee, S., Misra, A.A., Calvès, G., Nemčok, M., 2017. *Tectonics of the Deccan Large Igneous Province*. Geological Society, London, Special Publications 445.
- Müller, R.D., Seton, M., Zahirovic, S., Williams, S.E., Matthews, K.J., Wright, N.M., Shephard, G.E., Malone, K.T., Barnett-Moore, N., Hosseinpour, M., Bower, D.J., Cannon, J., 2016. Ocean basin evolution and global-scale plate reorganization events since Pangea breakup. *Annual Reviews of Earth and Planetary Sciences* 44:107–138. <http://dx.doi.org/10.1146/annurev-earth-060115-012211>.
- Müller, R.D., Hassan, R., Gurnis, M., Flament, N., Williams, S.E., 2018. Dynamic topography of passive continental margins and their hinterlands since the Cretaceous. *Gondwana Research* 53, 225–251 (in this issue).
- Nerlich, R., Colli, L., Ghelichkhani, S., Schuberth, B., Bunge, H.-P., 2016. Constraining central Neo-Tethys Ocean reconstructions with mantle convection models. *Geophysical Research Letters* 43:9595–9603. <http://dx.doi.org/10.1002/2016gl070524>.
- Oldroyd, D., 2013. Maps as pictures or diagrams: the early development of geological maps. *Rethinking the Fabric of Geology*. Geological Society Of America Special Paper 502, pp. 41–101.
- Peate, D.W., 1997. The Paraná-Etendeka Province. *Large Igneous Provinces: Continental, Oceanic, and Planetary Flood Volcanism*. pp. 217–245.
- Pierce, K.L., Morgan, L.A., 1992. The track of the Yellowstone hot spot: volcanism, faulting, and uplift. *Geological Society of America Memoirs* 179, 1–54.
- Pierce, K.L., Morgan, L.A., Saltus, R.W., 2002. Yellowstone plume head: postulated tectonic relations to the Vancouver slab, continental boundary and climate. In: Bonnichsen, B., White, C.M., McCurry, M. (Eds.), *Tectonic and Magmatic Evolution of the Snake River Plain Volcanic Province*. Idaho Geological Survey Bulletin Vol. 30, pp. 5–33.
- Pitman III, W.C., 1978. Relationship between eustacy and stratigraphic sequences of passive margins. *Geological Society of America* 89:1389–1403. [http://dx.doi.org/10.1130/0016-7606\(1978\)89<1389:RBEASS>2.0.CO;2](http://dx.doi.org/10.1130/0016-7606(1978)89<1389:RBEASS>2.0.CO;2).
- Pitman III, W.C., Golovchenko, X., 1991. Modelling sedimentary sequences. In: Müller, D.W., McKenzie, J.A., Weissert, H. (Eds.), *Controversies in Modern Geology (Proceedings of the HSU Symposium)*. Academic Press, London, pp. 279–309.
- Prenzel, J., Lisker, F., Monsees, N., Balestrieri, M.L., Läufel, A., Spiegel, C., 2018. Development and inversion of the Mesozoic Victoria Basin in the Terra Nova Bay (Transantarctic Mountains) derived from thermochronological data. *Gondwana Research* 53, 110–128 (in this issue).
- Prothero, D.R., Schwab, F., 2014. *Sedimentary Geology. An Introduction to Sedimentary Rocks and Stratigraphy*. Macmillan Learning (500 pp).
- Rainbird, R.H., Ernst, R.E., 2001. The sedimentary record of mantle-plume uplift. In: Ernst, R.E., Buchan, K.L. (Eds.), *Mantle Plumes: Their Identification Through Time*. Geological Society of America Special Paper Vol. 352:pp. 227–245. <http://dx.doi.org/10.1130/0-8137-2352-3.227>.
- Reed, J.C., Wheeler, J.O., Tucholke, B.E., 2005. *Geological Map of North America*. The Geological Society of America, Boulder, Colorado.
- Reidel, S.P., Camp, V.E., Tolan, T.L., Martin, B.S., 2013. The Columbia River flood basalt province: stratigraphy, areal extent, volume, and physical volcanology. *The Geological Society of America Special Paper* 497:1–43. [http://dx.doi.org/10.1130/2013.2497\(01](http://dx.doi.org/10.1130/2013.2497(01)).
- Ricard, Y., Fleitout, L., Froidevaux, C., 1984. Geoid heights and lithospheric stresses for a dynamic earth. *Annales Geophysicae* 2, 267–286.
- Richards, M.A., Engebretson, D.C., 1992. Large-scale mantle convection and the history of subduction. *Nature* 355:437–440. <http://dx.doi.org/10.1038/355437a0>.
- Richards, M.A., Hager, B.H., 1984. Geoid anomalies in a dynamic earth. *Journal of Geophysical Research* 89:5987–6002. <http://dx.doi.org/10.1029/JB089iB07p05987>.
- Richards, F.D., Hoggard, M.J., White, N.J., 2016. Cenozoic epiregiony of the Indian peninsula. *Geochemistry, Geophysics, Geosystems* 17 (12):4920–4954. <http://dx.doi.org/10.1002/2016GC006545>.
- Ritsema, J., Deuss, A., van Heijst, H.J., Woodhouse, J.H., 2011. S4ORTS: a degree-40 shear-velocity model for the mantle from new Rayleigh wave dispersion, teleseismic traveltimes, and normal-mode splitting function measurements. *Geophysical Journal International* 184:1223–1236. <http://dx.doi.org/10.1111/j.1365-246X.2010.04884.x>.
- Rowley, D.B., 2017. Earth's constant mean elevation: implication for long-term sea level controlled by oceanic lithosphere dynamics in a Pitman world. *The Journal of Geology* 125 (2), 141–153.
- Royden, L., Sclater, J.G., von Herzen, R.P., 1980. Continental margin subsidence and heat flow: important parameters in formation of petroleum hydrocarbons. *AAPG Bulletin* 64 (2), 173–187.
- Sahu, H.S., Raab, M.J., Kohn, B.P., Gleadow, A.J.W., Kumar, D., 2013. Denudation history of eastern Indian peninsula from apatite fission track analysis: linking possible plume-related uplift and the sedimentary record. *Tectonophysics* 608:1413–1428. <http://dx.doi.org/10.1016/j.tecto.2013.06.002>.
- Salvador, A. (Ed.), 1994. *International Stratigraphic Guide: A Guide to Stratigraphic Classification, Terminology, and Procedure (No. 30)*. Geological Society of America and the International Union of Geological Sciences <http://dx.doi.org/10.1130/9780813774022> (214 pp).
- Saunders, A.D., Jones, S.M., Morgan, L.A., Pierce, K.L., Widdowson, M., Xu, Y.G., 2007. Regional uplift associated with continental large igneous provinces: the roles of mantle plumes and the lithosphere. *Chemical Geology* 241:282–318. <http://dx.doi.org/10.1016/j.chemgeo.2007.01.017>.
- Schaber, K., Bunge, H.-P., Schuberth, B.S.A., Malservisi, R., Horbach, A., 2009. Stability of the rotation axis in high-resolution mantle circulation models: weak polar wander despite strong core heating. *Geochemistry, Geophysics, Geosystems* 10. <http://dx.doi.org/10.1029/2009GC002541>.
- Schäfer-Weiss, D., Veresmann, J., 2005. The influence of Goethe's Farbenlehre on early geological map colouring: Goethe's contribution to Christian Keferstein's General Charte von Teutschland (1821). *Imago Mundi* 57 (2):164–184. <http://dx.doi.org/10.1080/03085690500094990>.
- Schuberth, B.S.A., Bunge, H.-P., Steinle-Neumann, G., Moder, C., Oeser, J., 2009a. Thermal versus elastic heterogeneity in high-resolution mantle circulation models with pyrolite composition: high plume excess temperatures in the lowermost mantle. *Geochemistry, Geophysics, Geosystems* 10. <http://dx.doi.org/10.1029/2008GC002235>.
- Schuberth, B.S.A., Bunge, H.-P., Ritsema, J., 2009b. Tomographic filtering of high-resolution mantle circulation models: can seismic heterogeneity be explained by temperature alone? *Geochemistry, Geophysics, Geosystems* 10 (5). <http://dx.doi.org/10.1029/2009GC002401>.
- Sehrt, M., Glasmaier, U.A., Stockli, D.F., Labour, H., Kluth, O., 2018. The southern Moroccan passive continental margin: an example of differentiated long-term landscape evolution in Gondwana. *Gondwana Research* 53, 129–144 (in this issue).
- Sengör, A.M.C., 1995. Sedimentation and tectonics of fossil rifts. *Tectonics of Sedimentary Basins* 579, 53–118.
- Sengör, A.M.C., 2001. Elevation as indicator of mantle-plume activity. In: Ernst, R.E., Buchan, K.L. (Eds.), *Mantle Plumes: Their Identification Through Time*. Geological Society of America Special Papers Vol. 352:pp. 183–225. <http://dx.doi.org/10.1130/0-8137-2352-3.183>.
- Sengör, A.M.C., 2003. The large-wavelength deformations of the lithosphere. Materials for a history of the evolution of thought from the earliest times to plate tectonics. *Geological Society of America Memoirs* 347.
- Sengör, A.M.C., 2016. What is the use of the history of geology to a practicing geologist? The propaedeutical case of stratigraphy. *Journal of Geology* 124:643–698. <http://dx.doi.org/10.1086/688609>.
- Simmons, N.A., Forte, A.M., Grand, S.P., 2009. Joint seismic, geodynamic and mineral physical constraints on three-dimensional mantle heterogeneity: implications for the relative importance of thermal versus compositional heterogeneity. *Geophysical Journal International* 177:1284–1304. <http://dx.doi.org/10.1111/j.1365-246X.2009.04133.x>.
- Sinha, R., Kettanah, Y., Gibling, M.R., Tandon, S.K., Jain, M., Bhattacharjee, P.S., ... Ghazanfari, P., 2009. Craton-derived alluvium as a major sediment source in the Himalayan Foreland Basin of India. *Geological Society of America Bulletin* 121 (11–12), 1596–1610.
- Sleep, N.H., 1990. Hotspots and mantle plumes: some phenomenology. *Journal of Geophysical Research* 95:6715–6736. <http://dx.doi.org/10.1029/JB095iB05p06715>.
- Sleep, N.H., 1997. Lateral flow and ponding of starting plume material. *Journal of Geophysical Research* 102:10001–10012. <http://dx.doi.org/10.1029/97JB00551>.
- Sloss, L.L., 1963. Sequences in the cratonic interior of North America. *The Geological Society of America Bulletin* 74:93–113. [http://dx.doi.org/10.1130/0016-7606\(1963\)74\[93:SITCIO\]2.0.CO;2](http://dx.doi.org/10.1130/0016-7606(1963)74[93:SITCIO]2.0.CO;2).
- Sloss, L.L., 1992. Tectonic episodes of cratons: conflicting North America concepts. *Terra Nova* 4:320–328. <http://dx.doi.org/10.1111/j.1365-3121.1992.tb00821.x>.
- Sloss, L.L., Krumbein, W.C., Dapples, E.C., 1949. Integrated facies analysis. In: Longwell, C.R. (Ed.), *Sedimentary Facies in Geologic History*. Geological Society of America Memoir Vol. 39, pp. 91–124.
- Smith, W., 1816. *Strata Identified by Organized Fossils, Containing Prints of the Most Characteristic Specimens in Each Stratum* (London (1816–1819), 94 pp).
- Spasovic, S., Liu, L., Gurnis, M., 2009. Adjoint models of mantle convection with seismic, plate motion, and stratigraphic constraints: North America since the late Cretaceous. *Geochemistry, Geophysics, Geosystems* 10. <http://dx.doi.org/10.1029/2008GC002345>.
- Steckler, M.S., Watts, A.B., Thorne, J.A., 1988. Subsidence and basin modeling at the US Atlantic passive margin. *The Geology of North America* DNAG 2, 399–416.
- Stein, C.A., Stein, S., Merino, M., Randy Keller, G., Flesch, L.M., Jurdy, D.M., 2014. Was the Midcontinent Rift part of a successful seafloor-spreading episode? *Geophysical Research Letters* 41 (5):1465–1470. <http://dx.doi.org/10.1002/2013GL059176>.
- Steno, N., 1669. *De solido intra solidum naturaliter contento dissertationis prodromus: Florentia. Maer 2 (27)*, 181–227.
- Stille, H., 1919. Die Begriffe Orogenese und Epirogenese. *Zeitschrift der Deutschen Geologischen Gesellschaft* 71, 164–208.
- Stille, H., 1924. Kanon der Strandverschiebungen in Grundfragen der Vergleichenden Tektik. Verlag Gebrüder Bornträger, Berlin (443 pp).
- Stockli, D.F., 2000. *Regional Timing and Spatial Distribution of Miocene Extension in the Northern Basin and Range Province*. Ph.D. dissertation. Stanford University.
- Suess, E., 1883. *Das Antlitz der Erde*. 3rd ed. F. Tempsky, Vienna (778 pp. (1909)).
- Thiessen, R., Burke, K., Kidd, W.S.F., 1979. African hotspots and their relation to the underlying mantle. *Geology* 7, 263–266.
- Todal, A., Edholm, O., 1998. Continental margin off Western India and Deccan Large Igneous Province. *Marine Geophysical Research* 20:273–291. <http://dx.doi.org/10.1023/A:1004640508371>.
- Vail, P.R., Mitchum Jr., R.M., Thompson, S., 1977. *Seismic Stratigraphy and Global Changes of Sea Level: Part 4. Global Cycles of Relative Changes of Sea Level: Section 2. Application of Seismic Reflection Configuration to Stratigraphic Interpretation*. Bulletin of the American Association of Petroleum Geologists Special Volumes pp. 83–97.
- Vibe, J., Bunge, H.-P., Clark, S.R., 2018. Anomalous subsidence history of the West Siberian Basin as an indicator for episodes of mantle induced dynamic topography. *Gondwana Research* 53, 99–109 (in this issue).
- Wandrey, C.J., Law, B.E., 1999. *Maps showing geology, oil and gas fields and geologic provinces of South Asia*. US Geological Survey Open-File Report 97-470C, version 2, one CD-ROM.

- Walker, J.D., Geissman, J.W., Bowring, S.A., Babcock, L.E., 2013. The Geological Society of America Geologic Time Scale. *Geological Society of America Bulletin* <http://dx.doi.org/10.1130/B30712.1>.
- Walsh, S.L., Gradstein, F.M., Ogg, J.G., 2004. History, philosophy, and application of the Global Stratotype Section and Point (GSSP). *Lethaia* 37:201–218. <http://dx.doi.org/10.1080/00241160410006500>.
- Weismüller, J., Gmeiner, B., Ghelichkhan, S., Huber, M., John, L., Wohlmuth, B., Rüde, U., Bunge, H.-P., 2015. Fast asthenosphere motion in high resolution global mantle flow models. *Geophysical Research Letters* 42 (18):7429–7435. <http://dx.doi.org/10.1002/2015GL063727>.
- Weltje, G.J., von Eynatten, H., 2004. Quantitative provenance analysis of sediments: review and outlook. *Sedimentary Geology* 171 (1), 1–11.
- Wernicke, B., 1981. Low-angle normal faults in the basin and Range Province: nappe tectonics in an extending orogen. *Nature* 291:645–648. <http://dx.doi.org/10.1038/291645a0>.
- Wernicke, B., 2011. The California River and its role in carving Grand Canyon. *Geological Society of America Bulletin* 123 (7–8), 1288–1316.
- Wheeler, H.E., 1958. Time-stratigraphy. *Bulletin of the American Association of Petroleum Geologists* 41, 1045–1063.
- Wheeler, H.E., 1959. Stratigraphic units in space and time. *American Journal of Science* 257 (10), 692–706.
- Wheeler, H.E., 1964. Baselevel, lithosphere surface, and time-stratigraphy. *Geological Society of America Bulletin* 75 (7), 599–610.
- White, N., McKenzie, D., 1988. Formation of the “steer’s head” geometry of sedimentary basins by differential stretching of the crust and mantle. *Geology* 16:250–253. [http://dx.doi.org/10.1130/0091-7613\(1988\)016<250:FOTSSH>2.3.CO;2](http://dx.doi.org/10.1130/0091-7613(1988)016<250:FOTSSH>2.3.CO;2).
- Wilson, J.T., 1963. A possible origin of the Hawaiian islands. *Canadian Journal of Physics* 41 (6):863–870. <http://dx.doi.org/10.1139/p63-094>.
- Wilson, J.T., 1965. A new class of faults and their bearing on continental drift. *Nature* 207, 343–347.
- Wilson, J.T., 1966. Did the Atlantic close and then re-open? *Nature* 211:676–681. <http://dx.doi.org/10.1038/211676a0>.
- Ziegler, P.A., 1990. *Geological Atlas of Western and Central Europe*. 2nd ed. Shell Internationale Petroleum Maatschappij B.V. (239 pp. With enclosures).